Journal of
METAMORPHIC GEOLOGY

J. metamorphic Geol., 2016, **34,** 147–166 doi:10.1111/jmg.12176

The Plankogel detachment of the Eastern Alps: petrological evidence for an orogen-scale extraction fault

S. SCHORN* AND K. STÜWE
Institute of Earth Sciences, University of Graz, Universitätsplatz 2, A-8010, Graz, Austria (simon.schorn@hotmail.com)

ABSTRACT The so-called Plankogel detachment is an east-west trending, south-dipping low-angle structure that juxtaposes the high-*P* rocks of the eclogite type locality of the eastern European Alps against amphibolite facies rocks to the south. It occurs in both the Saualpe and Koralpe Complex in eastern Austria. During Cretaceous intracontinental subduction, the footwall and the hangingwall units of the Plankogel detachment were buried to different crustal levels as inferred by pseudosection modelling and conventional thermobarometry: ~23–24 kbar and 640–690 °C for the eclogite facies units in the footwall of the detachment and ~12–14 kbar and 550–580 °C for the amphibolite facies metapelites in the hangingwall. Despite the different peak metamorphic conditions, both sides of the detachment display a common overprint at conditions of ~10 kbar and 580–650 °C. From this, we infer a two-stage exhumation process and suggest that this two-stage process is best interpreted tectonically in terms of slab extraction during Eoalpine subduction. The first stage of exhumation occurred due to the downward (southward) extraction of a lithospheric slab that was localized in the trace of the Plankogel detachment. The later stage, however, is attributed to more regional erosion- or extension-driven processes. Since the Plankogel detachment is geometrically related to a crustal-scale shear zone further north (the Plattengneiss shear zone), we suggest that both structures are part of the same extraction fault system along which the syn-collisional exhumation of the Eoalpine high-*P* units of the Eastern Alps occurred. The suggested model is consistent with both the mylonitic texture of the Plattengneiss shear zone and the overall ambiguous shear sense indicators present in the entire region.

Key words: extraction fault; Plankogel detachment; Plattengneiss; Saualpe; slab extraction.

INTRODUCTION

High- to ultrahigh pressure metamorphic rocks are widespread in collisional orogens such as the European Alps. Eclogite facies rocks are commonly attributed to burial in subduction zones and their presence at the Earth's surface implies subsequent exhumation from depths of 70 km and more. Despite the many models proposed for the ascent of crustal material, the exact mechanisms remain under debate. For example, exhumation by the downward removal of slabs in connection with extraction faults (Froitzheim *et al.*, 2003, 2006; Janák *et al.*, 2004, 2006, 2015) is a recently proposed scenario. Extraction faults form due to the extraction of blocks from conjugated pairs of shears (Froitzheim *et al.*, 2006). They are characterized by (i) opposing shear sense in foot- and hangingwall, (ii) a loss of material between their margins and they involve (iii) a two-stage exhumation process. Extraction faults may occur on all scales (Froitzheim *et al.*, 2006). While orogeny-scale extraction faults are plausible structures in connection with exhumation mechanisms, representative examples on this scale have rarely been reported. Froitzheim *et al.* (2006) described the Combin fault in the Penninic Alps as a major metamorphic discontinuity which juxtaposes high-*P* rocks in the footwall to low-*P* rocks in the hangingwall. Thereby a discontinuity in recorded metamorphic pressures is evident which increases gradually towards the subducting slab that the authors attribute to the downward extraction of a sliver consisting of dense, mainly oceanic material. These authors argue that the Combin fault may be an example of an extraction fault.

In this contribution, we describe evidence from the Austroalpine Nappe Complex that suggests that the Plankogel detachment of the Eastern Alps (Fig. 1) may be a major extraction fault active during Late Cretaceous subduction. The Plankogel detachment is an east-west striking and southward dipping structure that separates the highest-grade metamorphic rocks of the Austroalpine Nappe Complex from lower-grade units (Fig. 1b,c) near the eclogite type locality in the Saualpe–Koralpe area (Haüy, 1822). Several authors, including Gregurek *et al.* (1997), Kurz *et al.* (2002) and Wiesinger *et al.* (2006), also recognized a major discontinuity in peak metamorphic conditions experienced by the foot- and hangingwall of the Plankogel detachment in both the Koralpe and Saualpe and suggested the Plankogel structure to be a 'low-angle normal fault'. Contrary to the nature of a normal fault,

**Present address*: Department of Geological Sciences, University of Cape Town, Private Bag, Rondebosch 7701, South Africa.

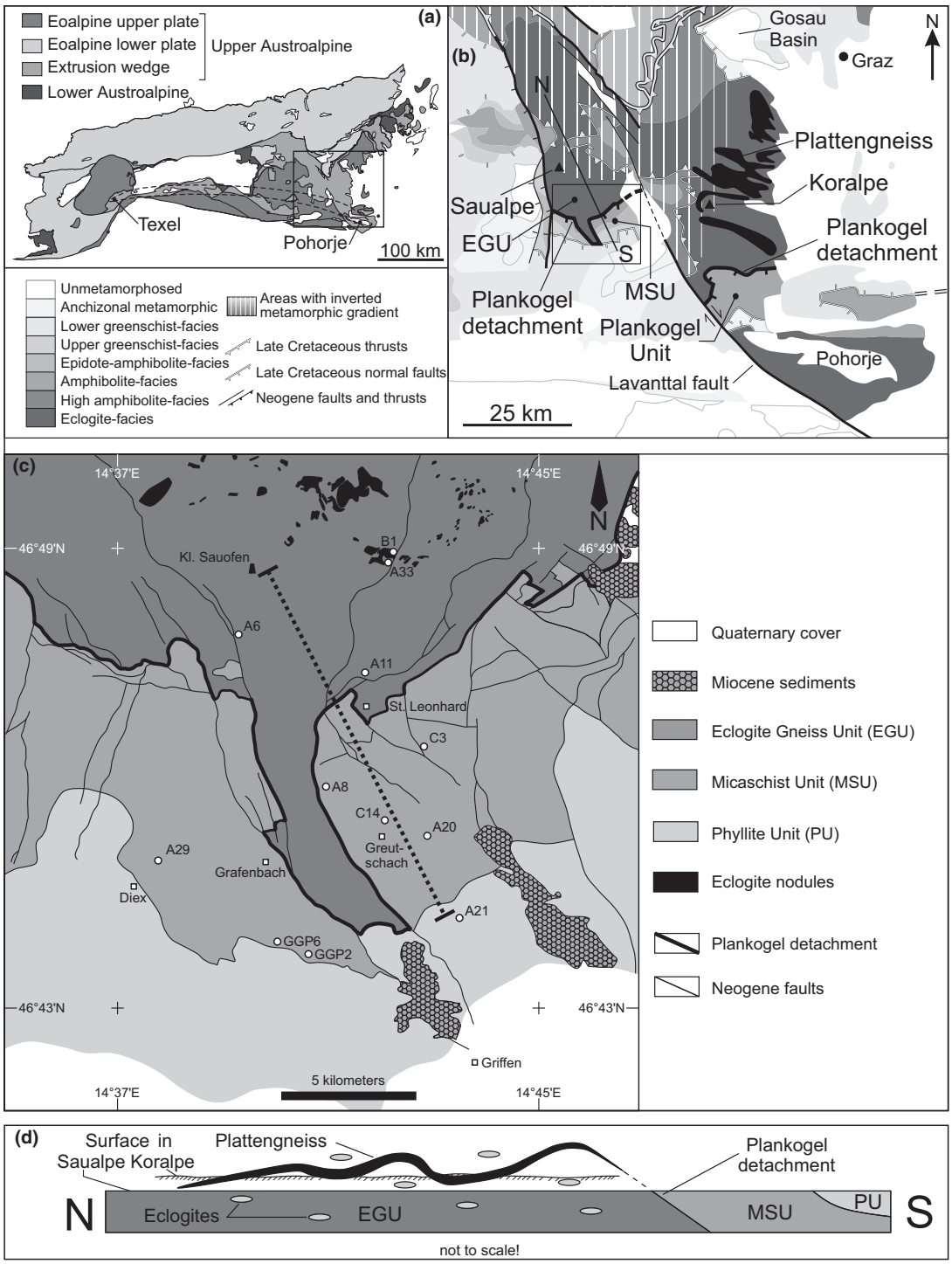

Fig. 1. Location map of the Plankogel detachment in the Eastern Alps. (a) Simplified geological map of the major tectonic units in the Eastern Alps (modified after Schmid *et al*., 2004) with approximate location of the Eoalpine high-*P* belt indicated by the dotted line. The box corresponds to the zoom-in shown in (b). Simplified geological map of the Saualpe–Koralpe area showing the metamorphic grade and major structures (modified after Froitzheim *et al*., 2008). The approximate location of the Plattengneiss in the Koralpe is shown in black (modified after Putz *et al*., 2006). The box matches to the zoom-in shown in (c). Simplified geological map showing the investigated area and sample localities. The dotted black line represents the transect on which the reported *P–T* data have been projected orthogonally (modified after the geological map of the Saualpe, Weissenbach *et al*., 1978). (d) North–south cartoon section through the investigated area along the profile shown in (b). In relation to the Koralpe Complex, it displays the hypothesized location of the Plattengneiss shear zone, now eroded away in the Saualpe (modified after Putz *et al*., 2006).

the evidence presented here suggests a new kinematic interpretation for the Plankogel structure. To avoid misleading terminology we refer here to the Plankogel structure as a 'detachment'. Our evidence is based on differences between structural separation and peak pressures recorded in units that are separated by the Plankogel detachment, as well as a common metamorphic overprint at a comparable crustal level for units in the foot- and hangingwall. Since previous petrological studies on the Plankogel detachment in the Koralpe region have already been described by other authors (Gregurek *et al*., 1997; Tenczer & Stüwe, 2003; Eberlei *et al*., 2014), the focus of this work is put on the Saualpe transect across the detachment.

GEOLOGICAL SETTING

The Plankogel detachment represents the southern limit of the eclogite facies Saualpe–Koralpe Complex of the Eastern Alps (Fig. 1b,c). In the Koralpe, it forms the tectonic contact between the eclogite facies Koralm Complex and the amphibolite grade units known as the Plankogel Unit in the southern Koralpe (Gregurek *et al*., 1997). An equivalent contact (here also referred to as the 'Plankogel detachment') is present in the southern Saualpe Complex. It is thought to have played a major role during the Eoalpine subduction and the subsequent exhumation of high-*P* units in both the Saualpe and the Koralpe (e.g. Wiesinger *et al*., 2006).

The polymetamorphic Saualpe Complex is part of the Koralpe-Wölz high-*P* Nappe system (Schmid *et al*., 2004; Thöni *et al*., 2008) and includes eclogites from gabbroic protoliths of Permian age embedded mostly in paragneisses (Thöni & Jagoutz, 1992; Miller & Thöni, 1997; Miller *et al*., 2007). The gabbros originated from lithospheric thinning related to the rifting and opening of the Meliata-Hallstatt oceanic domain (e.g. Thöni & Jagoutz, 1992). During the Permian, the region experienced metamorphism with peak conditions of 3.8–6.5 kbar and 600–650 °C (Habler & Thöni, 2001). Garnet whole-rock Sm/Nd isochrons from the northern Saualpe yield 267 ± 17 Ma for this event (Schuster *et al*., 2001). The Permian metamorphism was related to extensional lithospheric thinning (Habler & Thöni, 2001). Stüwe & Schuster (2010) argued that this thinning led to a thermal sag-stage subsidence during the Mesozoic, which was followed by the deposition of thick Triassic sediments. This ultimately resulted in negative buoyancy of the lithosphere which caused the onset of the Eoalpine intracontinental subduction in the Late Cretaceous. The subduction triggered the Eoalpine high-*P*–low-*T* metamorphism which overprinted the Permian precursor units. The Cretaceous event commenced at *c*. 95–94 Ma and ceased between 90 and 88 Ma. Peak conditions of 22 ± 2 kbar and 630–740 °C were reached (Thöni *et al*., 2008). The Eoalpine high-*P* belt, which extends for ~350 km from the Texel Complex in the west to the Pohorje Mountains in the east, is interpreted as the trace of this subduction zone (Thöni & Jagoutz, 1993; Fig. 1a). Structurally inverted and upright parts occur particularly in the Saualpe–Koralpe area (Fig. 1b), suggesting that the suture of the Eoalpine subduction zone is localized between (Stüwe & Schuster, 2010). The Eoalpine event was followed by rapid exhumation and cooling (Wiesinger *et al*., 2006). Today, the Saualpe Complex is separated from the Koralpe Complex by the dextral Lavanttal fault system that was active in the Early Miocene, between 18 and 16 Ma (e.g. Kurz *et al*., 2011; Fig. 1b). This fault zone offsets the Plankogel detachment by some 15 km with a minor vertical displacement which caused the Saualpe Complex to expose slightly deeper crustal levels than the Koralpe (Legrain *et al*., 2014).

The Plankogel detachment in the southern Saualpe juxtaposes the Eclogite Gneiss Unit (EGU) that constitutes the majority of the Saualpe in the footwall to the Micaschist Unit (MSU) in the hangingwall (Wiesinger *et al*., 2006). The structurally lowermost part of the MSU consists of analogous lithologies (mostly metapelites and amphibolites) that occur in the type locality for the Plankogel Unit in the northwestern Saualpe (Fritsch *et al*., 1960). Pilger & Schönenberg (1975) recognized roughly north–south-directed stretching lineations on a generally flat-lying foliation throughout the Saualpe Complex, but also noted that overall shear sense is unclear. The flattening is interpreted to have occurred syn-metamorphically and is thought to have been followed by a late-stage warping of the crystalline units.

The MSU is structurally overlain by the greenschist facies Phyllite Unit (PU; Wiesinger *et al*., 2006), largely consisting of phyllites and marbles of Early Paleozoic depositional age (Neugebauer, 1970) (Fig. 3d). Here, we focus mainly on the units occurring in the foot- and hangingwall of the detachment in order to constrain the metamorphic history of the area and to unravel the role of the Plankogel detachment during the Eoalpine event. As we argue for a prominent role played by the Plankogel detachment in the Saualpe–Koralpe area, for tectonic context the Plattengneiss shear zone (PGSZ) in the Koralpe is also briefly described.

The Plattengneiss shear zone

The PGSZ is a major flat-lying mylonitic horizon of ~250–600 m thickness (Putz *et al*., 2006). Due to its geometry it is mainly exposed in the Koralpe region (Frank, 1987); however, equivalent high-strain rocks occur in the Saualpe area. Conspicuous north–south trending stretching lineations, as well as eclogite boudins, occur throughout the shear zone (e.g. Eberlei *et al*., 2014; Fig. 1d). The PGSZ consists of a single sheet and is slightly warped into a series of open syn- and antiforms (Putz *et al*., 2006). The syn-deforma-

Table 1. Sample localities.

Sample	Unit	Lithology	Latitude N	Longitude E
B1	EGU	Eclogite	46.818176	14.708558
A33	EGU	grt–bt–st–ky–micaschist	46.818366	14.703852
A6	EGU	grt–bt–st–ky–micaschist	46.801244	14.652068
A11	MSU	grt–bt–st–ky–micaschist	46.792397	14.694435
A29	MSU	grt–st–pg–chl–micaschist	46.749622	14.624976
A8	MSU	grt–st–cld–pg–chl–micaschist	46.766483	14.681342
C3	MSU	grt–bt–st–ky–micaschist	46.776555	14.714764
C14	MSU	grt–st–chl–pg–micaschist	46.758913	14.700909
A20	MSU	grt–bt–st–ky–micaschist	46.755133	14.715410
GGP6	MSU	grt–st–cld–pg–chl–micaschist	46.731111	14.665000
GGP2	MSU	grt–st–cld–pg–chl–micaschist	46.730833	14.675000

tional assemblages correspond to that of the EGU in the Saualpe and are characterized by Cretaceous-age deformation (e.g. Kurz *et al*., 2002). The PGSZ does not separate different tectonic units in its foot- and hangingwall (Roffeis, 2008). Several authors debated the interpretation of shear sense indicators based on different approaches (e.g. Kurz *et al*., 2002; Kurz & Fritz, 2003; Putz *et al*., 2006; Eberlei *et al*., 2014). Eberlei *et al*. (2014) suggested that the shear senses in the shear zone may be opposite in the foot- and hangingwall and that it constitutes a south-directed channel flow type extrusion. These authors also suggest that such a channel flow model implies a significant loss of material from within the shear zone, which is interpreted to have been extracted downwards (southwards) during subduction. This process led to a removal of significant amounts of eclogites, causing a reversal in buoyancy of the area that triggered rapid exhumation shortly after the extrusion (Eberlei *et al*., 2014). The southernmost outcrop of the PGSZ in the Koralpe is a shallow synform, which strikes out of the topography (Putz *et al*., 2006; Eberlei *et al*., 2014), but it is likely that it joins the Plankogel detachment in the south (Fig. 1d). As such, the PGSZ and the Plankogel detachment are probably part of the same major structure and we refer to it as the Plattengneiss-Plankogel shear system (PGPK). Since the Saualpe is exhumed marginally more with respect to the Koralpe, the flat-lying Plattengneiss horizon is likely to have been eroded there (Fig. 1d). Nevertheless, the rocks of the EGU are highly deformed with a similar non-unique shear sense as those of the Koralpe.

PETROGRAPHY AND MINERAL CHEMISTRY

In order to constrain the tectonic significance of the Plattengneiss-Plankogel shear system, a transect across the detachment in the southern Saualpe (Fig. 1c, Table 1) was sampled. Conventional thermobarometry was performed on the collected specimens, whereas pseudosection modelling was carried out on two representative samples of the foot- and hangingwall. Mineral chemical analyses were carried out on carbon-coated thin sections using a JEOL JSM 6310 scanning electron microscope at the Institute of Earth Sciences, University of Graz, Austria, equipped with a LINK ISIS energy dispersive system as well as a MICROSPEC wavelength dispersive system. Selected analyses and chemical mapping were carried out using a JEOL JXA 8200 electron microprobe at the Institute of Earth Sciences, Montanuniversity of Leoben, Austria. Measurement conditions were 15 kV acceleration voltage, 5 nA beam current and 2–3 μm spot size. A range of synthetic and natural mineral standards were employed for element calibration. Mineral formulae were calculated using the software PET 7 (Dachs, 1998). Whole-rock bulk compositions were determined on glassy discs with X-ray fluorescence (XRF) using a Bruker Pioneer S4, calibrated utilizing ~60 international reference materials, located at the Institute of Earth Sciences, University of Graz, Austria. For this, fresh chips of whole-rock samples were carefully selected, powdered and dried in an oven at ~105 °C for at least 2 h. 1 g of dried sample powder and 7 g dilithiumtetraborate was fused at ~1300 °C with a semi-automatic VAA-2 fusion machine from HD-Electronic. Mineral abbreviations are after Whitney & Evans (2010). Thin-section- and SEM photographs of representative samples are shown in Figs 2 & 3.

Footwall (EGU)

The Eclogite Unit in the footwall of the Plankogel detachment comprises the highest-grade rocks of the southern Saualpe Complex (Fig. 1c,d). It consists mainly of coarse-grained garnet micaschists and paragneisses with intercalated eclogite boudins, amphibolites and metapegmatites. The rocks are highly deformed; but – similar to the Koralpe – shear sense is commonly ambiguous. The metapelites of the EGU consist mainly of garnet + staurolite + kyanite + biotite + muscovite + plagioclase + quartz. Accessory phases are hematite, rutile (partly replaced by ilmenite), zoisite, apatite as well as rare monazite and zircon. Garnet exhibits weak growth-zoning patterns, whereas X_{Alm} increases (~0.60–0.66) and X_{Prp} decreases (~0.28–0.20) from core to rim. X_{Grs} displays a slight increase from the core (~0.10), whereas it increases towards the rim to a maximum of ~0.13 and finally drops again to core values at the outermost rim (Fig. 4c). Kyanite is present as aggregates of small (<0.1 mm), idioblastic grains and forms paramorphs after precursor

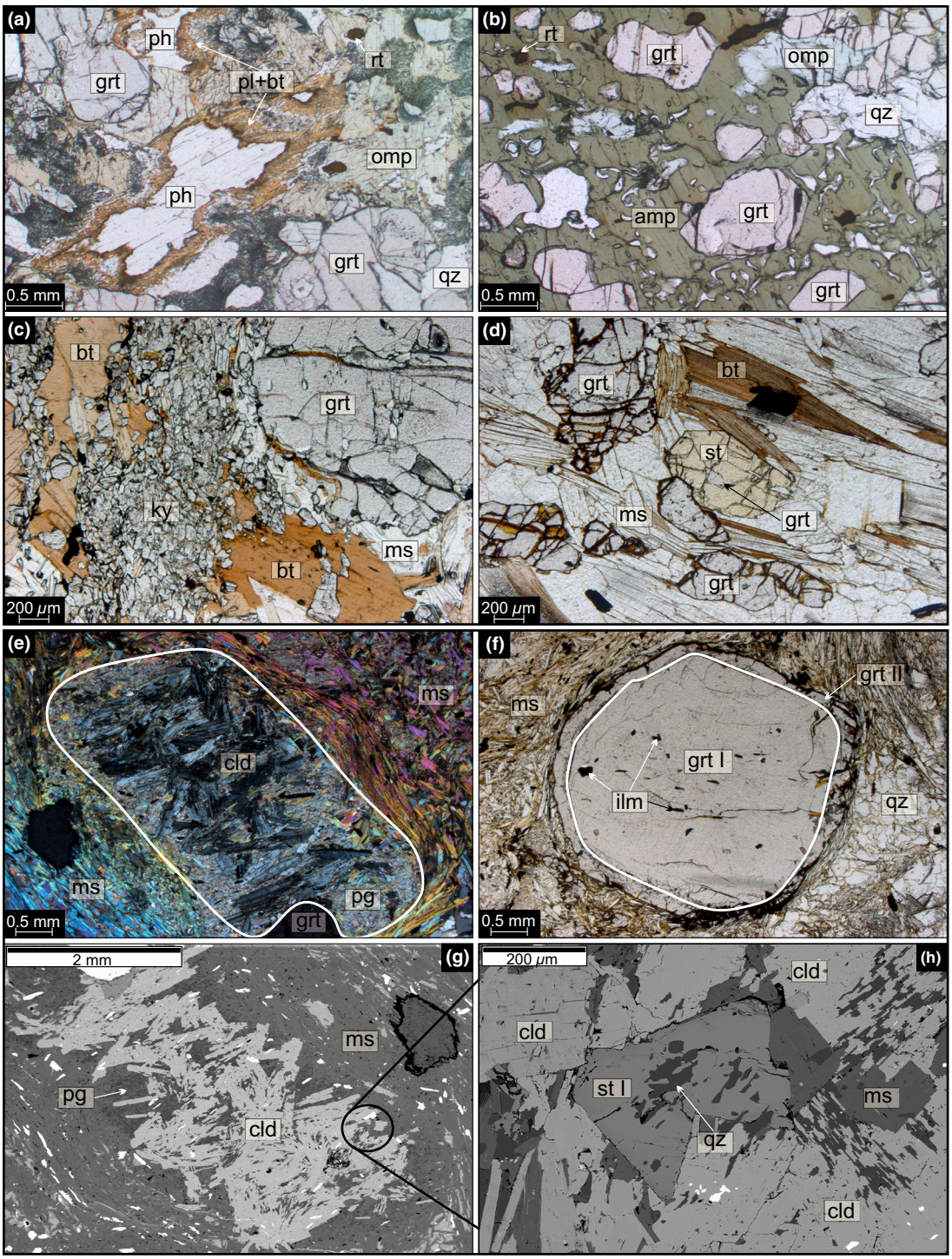

Fig. 2. Photomicrographs of representative samples showing phase- and microstructural relationships. (a)–(d) are from the footwall (Eclogite Gneiss Unit), (e)–(h) are from the hangingwall (Micaschist Unit). (a) Eclogite facies peak assemblage consisting of garnet, omphacite, phengite and quartz. Note the symplectitic intergrowth of amphibole/clinopyroxene + plagioclase around omphacite and plagioclase + biotite around phengite; sample B1. (b) Poikiloblastic hornblende overgrowing the primary assemblage in eclogite sample B3. (c) Hypidioblastic, fractured garnet, rich in quartz inclusions, in textural equilibrium with biotite, muscovite and fine-grained kyanite (paramorphs after Permian andalusite); sample A33. (d) Hypidioblastic staurolite with small garnet inclusion; sample A33. (e) Chloritoid pseudomorph in association with fine-grained paragonite and sericite; sample GGP6. Crossed polars. (f) Hypidioblastic two-phase zoned garnet; sample GGP6. (g) Back scatter-image of a chloritoid pseudomorph; sample GGP6. (h) Detail of (g) showing a relict staurolite inclusion (st I) inside the chloritoid pseudomorph; backscattered-electron image.

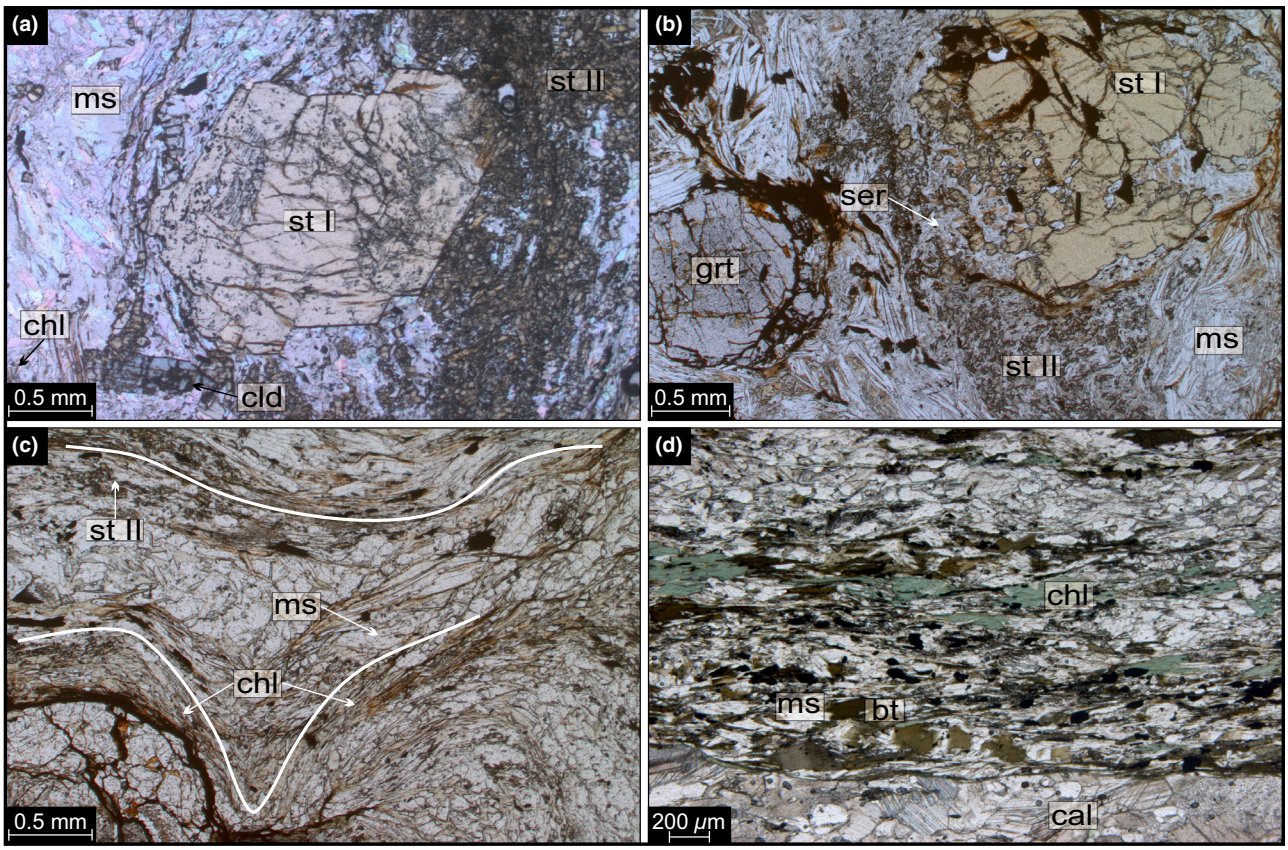

Fig. 3. Photomicrographs of representative samples from the Micaschist Unit (a–c) and the Phyllite Unit (d). (a) Idioblastic relict staurolite (st I) surrounded by fine-grained, idiomorphic staurolite (st II). (b) Hypidioblastic relict staurolite (st I) partly pseudomorphed by secondary sericite and surrounded by fine-grained staurolite (st II). (c) Equilibrium chlorite foliated with white mica and second generation staurolite (st II). The white lines trace the foliation developed during the last deformational stage. (d) Low-grade phyllite consisting of chlorite + biotite + white mica + calcite + quartz.

(Permian) andalusite (e.g. Pilger & Schönenberg, 1975; Habler & Thöni, 2001) (Fig. 2c). Kyanite also occurs as similarly sized inclusions in biotite (Fig. 2c). Staurolite is present as hypidioblastic grains with abundant inclusions of quartz and rarely of garnet (Fig. 2d). Poikiloblastic intergrowths of plagioclase, muscovite and biotite are rarely present. Chlorite grows around garnet and biotite, representing a late retrograde phase. The Koralpe area hosts equivalent rocks, referred to as the 'Hirschegg Gneiss' (Becker, 1976).

Representative eclogite samples are characterized by the assemblage garnet + omphacite + quartz + rutile ± amphibole ± phengite ± zoisite, with a diablastic texture (Fig. 2a). The investigated samples are largely undeformed to weakly deformed. Garnet is usually chemically homogeneous or shows slight prograde increase in X_{Prp} from core to rim (0.26–0.33). Based on microstructural and chemical analysis, at least two different amphibole generations can be distinguished: (i) an earlier generation of compositionally zoned poikiloblastic hornblende (Fig. 2b) (e.g. Massonne, 2012; Palin *et al.*, 2014) surrounding garnet and quartz or occurring as keliphitic rims around garnet and (ii) symplectites of amphibole, plagioclase and/or clinopyroxene around omphacite. Phengite with up to 3.3 Si p.f.u. occurs sporadically in the matrix. It is surrounded by fine-grained symplectitic intergrowths of plagioclase and biotite (Fig. 2a). Rutile is locally transformed to ilmenite. Representative mineral compositions are reported in Tables 2 and 3.

Hangingwall (MSU)

The MSU in the hangingwall of the Plankogel detachment (Fig. 1c,d) consists of foliated garnet micaschists, amphibolites and garnet amphibolites. In analogy to the Plankogel Unit in the northwestern Saualpe (Fritsch *et al.*, 1960; Thöni & Miller, 2009) and in the southern Koralpe (Gregurek *et al.*, 1997), true eclogites or retrogressed eclogites are notoriously absent in the MSU (see also Wiesinger *et al.*, 2006 for further details). The volumetrically dominant metapelites contain variable amounts of staurolite, chloritoid, biotite, plagioclase and kyanite, whereas two distinct mineral generations can be inferred by chemical and microstructural analysis (see Figs 2 & 3; Table 4). The first comprises hypidioblastic garnet

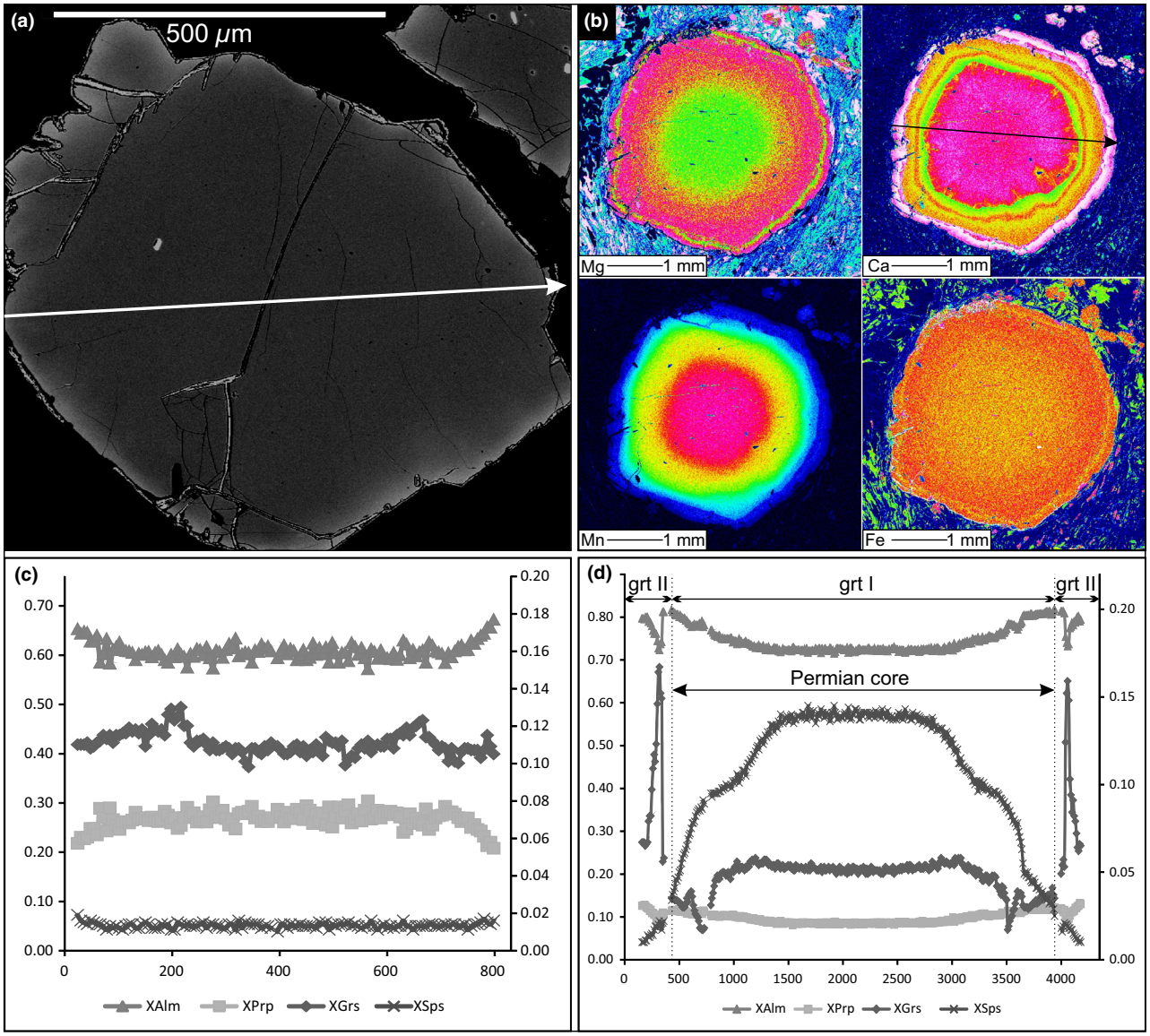

Fig. 4. Chemical maps and zoning profiles for garnet porphyroblasts from the footwall (Eclogite Gneiss Unit) (a and c) and the hangingwall (Micaschist Unit) (b and d). X_{Grs} and X_{Sps} refer to the scale to the right-hand of the diagram, X_{Alm} and X_{Prp} to the left-hand side. Scale is in microns. (a) Backscatter-image of a representative garnet from the footwall (EGU); sample A33. (b) Chemical map of major elements of complexly zoned polyphasic garnet, hangingwall (MSU); sample GGP6. (c) Chemical zoning profile along the trace shown in (a). (d) Chemical zoning profile along the trace indicated in (b).

cores with common inclusions of quartz, graphite and ilmenite (denoted as 'grt I' in Fig. 2f). Hypidioblastic staurolite up to 3 mm in size rich in quartz inclusions is also attributed to the earlier assemblage (referred to as 'st I' in Figs 2h & 3a,b). The second generation assemblage consists of garnet + staurolite + chloritoid + chlorite + muscovite + paragonite + quartz. Accessory phases are ilmenite, relict rutile, monazite, tourmaline and apatite. Locally fine-grained kyanite aggregates (interpreted as paramorphs after andalusite in analogy to the EGU), biotite and plagioclase occur with garnet, staurolite and muscovite. Common C-type shear band cleavage, rotated porphyroblasts and mica-fish textures indicate pervasive deformation with equally many top-to-the-south and top-to-the-north shear sense indicators in the MSU.

Garnet displays evidence for polyphasic growth. Ca-poor cores ($X_{Grs} \leq 0.06$) show a complex zoning pattern which is thought to be of Permian origin (e.g. Thöni & Miller, 2009) and is thus beyond the interest of this paper (denoted as 'grt I' in Fig. 2f and 'Permian core' in Figs 2h & 3a,b). The cores are commonly surrounded by discontinuous rims (referred to as 'grt II' in Figs 2f & 4d), whereas abrupt variations in the zoning pattern are evident. A sharp increase in

Table 2. Representative mineral compositions for eclogite sample B1 from the Eclogite Gneiss Unit in the footwall.

Phase	Garnet			Omphacite			Phengite			Amphibole		
Position	Core	Rim	Rim	Rim	Rim	Rim	Rim	Rim	Core	Rim	Rim	Rim
Label	B1_5grtcore	B1_3grt	B1_7grt	B1_17omph	B1_18omph	B1_19omph	B1_11wm	B1_13wm	B1_16wm	B1_26amph	B1_25amph	B1_29amph
SiO_2	39.34	39.38	39.33	56.47	56.43	56.91	50.13	49.75	50.15	43.00	43.46	44.50
TiO_2	0.21	b.d.l.	b.d.l.	0.15	0.15	0.21	0.86	0.88	0.85	0.65	0.57	1.13
Al_2O_3	21.49	22.36	21.98	10.84	11.05	11.04	31.08	30.83	30.51	15.39	16.94	14.23
Cr_2O_3	b.d.l.	0.08	b.d.l.	0.15	0.08	0.12	0.10	b.d.l.	b.d.l.	b.d.l.	b.d.l.	b.d.l.
FeO	21.88	23.13	22.48	3.48	3.50	3.53	1.22	1.15	1.12	10.66	10.64	8.84
MnO	0.35	0.37	0.34	b.d.l.	0.00	b.d.l.	0.00	b.d.l.	b.d.l.	b.d.l.	0.11	b.d.l.
MgO	6.74	7.61	7.77	9.17	9.04	8.78	3.05	3.13	3.18	12.80	11.29	13.40
ZnO	n.d	n.d	n.d	n.d	n.d	n.d	n.d	n.d	n.d	n.d	n.d	n.d
CaO	9.87	7.63	8.07	13.62	13.69	13.74	b.d.l.	b.d.l.	b.d.l.	9.92	8.96	10.45
Na_2O	n.d	n.d	n.d	5.93	5.72	5.89	1.02	1.16	1.06	3.33	3.80	2.98
K_2O	n.d	0.00	n.d	b.d.l.	b.d.l.	b.d.l.	9.77	9.68	9.63	0.98	0.88	1.04
Total	99.88	100.56	99.97	99.80	99.66	100.21	97.23	96.59	96.51	96.73	96.66	96.58
Oxygen	12	12	12	6	6	6	11	11	11	23	23	23
Si	3.02	3.00	3.01	2.00	2.00	2.01	3.26	3.25	3.28	6.31	6.35	6.47
Ti	0.01	0.00	0.00	0.00	0.00	0.01	0.04	0.04	0.04	0.07	0.06	0.12
Al	1.95	2.01	1.98	0.45	0.46	0.46	2.38	2.38	2.35	2.66	2.92	2.44
Cr	0.00	0.01	0.00	0.00	0.00	0.00	0.01	0.00	0.00	0.00	0.00	0.00
Fe^{2+}	1.41	1.47	1.44	0.10	0.10	0.10	0.07	0.06	0.06	1.31	1.30	1.08
Mn	0.02	0.02	0.02	0.00	0.00	0.00	0.00	0.00	0.00	0.00	0.01	0.00
Mg	0.77	0.86	0.89	0.48	0.48	0.46	0.30	0.31	0.31	2.80	2.46	2.90
Zn	0.00	0.00	0.00	0.00	0.00	0.00	0.00	0.00	0.00	0.00	0.00	0.00
Ca	0.81	0.62	0.66	0.52	0.52	0.52	0.00	0.00	0.00	1.56	1.40	1.63
Na	0.00	0.00	0.00	0.41	0.39	0.40	0.13	0.15	0.13	0.95	1.08	0.84
K	0.00	0.00	0.00	0.00	0.00	0.00	0.81	0.81	0.80	0.18	0.16	0.19
Total	7.99	8.00	8.00	3.97	3.96	3.96	6.98	7.00	6.98	15.84	15.74	15.67

Table 3. Representative mineral compositions for grt–bt–st–ky gneiss samples from the Eclogite Gneiss Unit in the footwall.

Sample	A33	A6	A33	A6	A33	A6	A33	A6	A33	A6
Phase	Garnet		Biotite		Staurolite		Plagioclase		Muscovite	
Position	Rim	Rim	Matrix	Matrix	Matrix	Matrix	Matrix	Matrix	Matrix	Matrix
Label	A33_2grt	A6_3grt	A33_12bi	A6_2bi	A33_6st	A6_2stau	A33_22plg	A6_4plg	A33_23wm	A6_4_17wm
SiO_2	38.08	36.82	37.32	36.65	27.75	28.10	60.87	62.42	46.93	46.90
TiO_2	b.d.l.	b.d.l.	1.52	1.66	0.62	0.56	n.d	n.d	0.47	0.74
Al_2O_3	21.09	20.95	19.12	19.11	53.19	54.16	24.65	24.09	36.40	34.78
Cr_2O_3	b.d.l.	b.d.l.	b.d.l.	b.d.l.	b.d.l.	b.d.l.	n.d	n.d	b.d.l.	b.d.l.
FeO	31.76	34.49	16.77	18.09	12.91	12.08	b.d.l.	b.d.l.	0.79	1.11
MnO	0.58	1.36	b.d.l.	b.d.l.	0.20	b.d.l.	n.d	n.d	b.d.l.	b.d.l.
MgO	4.82	3.34	11.10	11.00	1.76	1.61	n.d	n.d	0.61	1.17
ZnO	n.d	n.d	n.d	n.d	0.84	2.12	n.d	n.d	n.d	n.d
CaO	3.12	2.59	n.d	n.d	n.d	n.d	5.67	5.49	b.d.l.	b.d.l.
Na_2O	n.d	n.d	0.31	0.20	n.d	n.d	8.31	8.21	2.47	1.20
K_2O	n.d	n.d	8.87	9.02	n.d	n.d	0.11	0.10	7.78	9.46
Total	99.45	99.55	95.01	95.73	97.27	98.63	99.61	100.31	95.45	95.36
Oxygen	12	12	11	11	48	48	8	8	11	11
Si	3.03	2.97	2.79	2.74	7.75	7.75	2.71	2.75	3.08	3.10
Ti	0.00	0.00	0.09	0.09	0.13	0.12	0.00	0.00	0.02	0.04
Al	1.98	1.99	1.68	1.69	17.51	17.60	1.30	1.25	2.81	2.71
Cr	0.00	0.00	0.00	0.00	0.00	0.00	0.00	0.00	0.00	0.00
Fe^{2+}	2.11	2.25	1.05	1.13	3.02	2.79	0.00	0.00	0.04	0.06
Mn	0.04	0.09	0.00	0.00	0.05	0.00	0.00	0.00	0.00	0.00
Mg	0.57	0.40	1.24	1.23	0.73	0.66	0.00	0.00	0.06	0.12
Zn	0.00	0.00	0.00	0.00	0.17	0.43	0.00	0.00	0.00	0.00
Ca	0.27	0.22	0.00	0.00	0.00	0.00	0.27	0.26	0.00	0.00
Na	0.00	0.00	0.05	0.03	0.00	0.00	0.72	0.70	0.31	0.15
K	0.00	0.00	0.85	0.86	0.00	0.00	0.01	0.01	0.65	0.80
Total	7.99	7.93	7.73	7.77	29.36	29.34	5.00	4.97	6.98	6.98

X_{Grs} from ~0.05 to ~0.16 is accompanied by a drop in X_{Alm} (~0.80–0.70) and a drop in X_{Prp} (~0.12–0.09) (Table 4; Fig. 4b,d). The discontinuous variations of the major elements in the garnet zoning pattern indicate changes in metamorphic conditions. More precisely, these drastic chemical variations are interpreted as indication for the onset of the Eoalpine metamorphism. Following the discontinuous variations, the garnet compositions reach values close to those prior to the sharp changes. Note especially the pronounced drop in X_{Grs} from the maximum of ~0.16 to ~0.06. Coarse-grained garnet grains (up to

Table 4. Representative mineral compositions for metapelite samples from the Micaschist Unit in the hangingwall.

Lithology	Garnet–staurolite–chloritoid–paragonite micaschist													
Sample	GGP6		GGP2		GGP6	GGP2	GGP6	GGP2	GGP6	GGP2	GGP6	GGP2	GGP6	GGP2
Phase	Garnet				Staurolite		Chloritoid		Muscovite		Paragonite		Chlorite	
Position	Core	Rim	Core	Matrix	Matrix	Matrix	Matrix	Matrix	Matrix	Matrix	Matrix	Matrix	Matrix	Matrix
Label	L196GGP6	GGP6_2grt	GGP2_grtcore	GGP2_grt2	GGP6_8stau	GGP2_4st	GGP6_6ctd	GGP2_1ctd	GGP6_5wm	GGP2_7	GGP6_3OPa	GGP2_13pa	GGP6_6chl	GGP2_4_1
SiO_2	36.72	37.30	36.82	37.50	28.61	28.54	24.85	24.96	48.36	47.56	46.09	47.85	25.01	25.18
TiO_2	b.d.l.	b.d.l.	b.d.l.	b.d.l.	0.27	0.52	b.d.l.	b.d.l.	0.34	0.64	0.20	0.12	b.d.l.	b.d.l.
Al_2O_3	21.24	20.15	20.75	20.13	53.99	53.80	39.68	40.51	36.40	36.85	39.31	40.42	23.32	22.23
Cr_2O_3	b.d.l.	b.d.l.	b.d.l.	b.d.l.	0.15	b.d.l.	b.d.l.	b.d.l.	b.d.l.	b.d.l.	b.d.l.	b.d.l.	b.d.l.	b.d.l.
FeO	32.50	36.50	32.13	36.21	11.94	13.39	22.98	22.62	1.18	0.87	1.65	0.42	24.46	23.99
MnO	6.21	0.51	6.76	0.38	b.d.l.	0.12	b.d.l.	0.12	b.d.l.	b.d.l.	b.d.l.	b.d.l.	b.d.l.	b.d.l.
MgO	2.14	3.18	1.74	2.88	1.34	1.55	4.10	3.53	0.76	0.63	b.d.l.	0.30	14.80	15.73
ZnO	n.d	n.d	n.d	n.d	1.16	0.80	b.d.l.	b.d.l.	n.d	n.d	n.d	n.d	n.d	n.d
CaO	1.79	1.94	1.61	2.06	n.d	n.d	n.d	n.d	b.d.l.	b.d.l.	0.42	0.23	n.d	n.d
Na_2O	n.d	n.d	n.d	n.d	n.d	n.d	n.d	n.d	0.69	1.44	4.64	5.99	n.d	n.d
K_2O	n.d	n.d	n.d	n.d	n.d	n.d	n.d	n.d	8.52	8.88	3.00	1.43	n.d	n.d
Total	100.60	99.58	99.81	99.16	97.46	98.72	91.62	91.74	96.25	96.87	95.31	96.75	87.59	87.13
Oxygen	12	12	12	12	48	48	14	14	11	11	11	11	18	18
Si	2.96	3.02	3.00	3.04	7.92	7.85	1.03	1.03	3.13	3.08	2.98	3.01	2.62	2.11
Ti	0.00	0.00	0.00	0.00	0.06	0.11	0.00	0.00	0.02	0.03	0.01	0.01	0.00	0.00
Al	2.02	1.92	1.99	1.93	17.62	17.44	1.93	1.97	2.78	2.81	2.99	2.99	2.88	2.75
Cr	0.00	0.00	0.00	0.00	0.03	0.01	0.00	0.00	0.00	0.00	0.00	0.00	0.00	0.00
Fe^{2+}	2.12	2.43	2.18	2.46	2.77	3.08	0.77	0.78	0.06	0.05	0.09	0.02	2.14	2.11
Mn	0.42	0.04	0.47	0.03	0.00	0.03	0.00	0.00	0.00	0.00	0.00	0.00	0.00	0.00
Mg	0.26	0.38	0.21	0.35	0.55	0.64	0.00	0.22	0.07	0.06	0.00	0.03	2.31	2.46
Zn	0.00	0.00	0.00	0.00	0.24	0.16	0.25	0.00	0.00	0.00	0.00	0.00	0.00	0.00
Ca	0.16	0.17	0.14	0.18	0.00	0.00	0.00	0.00	0.00	0.00	0.03	0.02	0.00	0.00
Na	0.00	0.00	0.00	0.00	0.00	0.00	0.00	0.00	0.09	0.18	0.58	0.73	0.00	0.00
K	0.00	0.00	0.00	0.00	0.00	0.00	0.00	0.00	0.70	0.73	0.25	0.12	0.00	0.00
Total	7.94	8.00	8.00	7.98	29.19	29.32	4.00	3.99	6.85	6.94	6.93	6.92	9.94	9.43

5 mm in diameter) show the most dramatic major- and trace element zoning, although similar patterns exist in every garnet studied. Between the aforementioned Ca-poor core and the Ca-rich rim of second garnet generation a thin layer rich in Fe–Ti oxides is present. Relict staurolite (st I) is commonly surrounded by fine-grained (micron-sized) inclusion-free aggregates of idioblastic staurolite of a probably later generation (denoted as 'st II' in Fig. 3a,b). Despite the clear microstructural difference, the two generations show comparable compositions. Relict staurolite is also commonly pseudomorphically replaced by fine-grained sericite to variable extents (Fig. 3b). A first generation of chlorite with weak pleochroism occurs in the foliation along with white mica (Fig. 3c). Secondary, pleochroic chlorite is commonly present around the margins of garnet.

A conspicuous specimen of the hangingwall (sample GGP6), a garnet-staurolite-chloritoid-chlorite micaschist, hosts large up to 8 mm, prismatic-shaped idioblastic clots pseudomorphed by chloritoid with no preferred orientation (Fig. 2e, g). Inside the pseudomorphs fine-grained Na-rich paragonite and sericite are common as well as small staurolite of second generation that displays straight grain boundaries when in contact with chloritoid (Fig. 2h). Both phases also occur as idiomorphic porphyroblasts in the matrix and are in clear textural equilibrium. Representative mineral compositions are reported in Table 4.

The MSU is structurally overlain by the PU, which consists of foliated biotite-chlorite-calcite bearing phyllites (Fig. 3d) and marbles. The notably lower metamorphic grade (greenschist facies) indicates that the PU was not involved in the Cretaceous subduction-related metamorphism and is therefore not considered further.

In the southern Saualpe area a polymetamorphic evolution is indicated by the occurrence of microstructurally and compositionally distinct mineral generations. The first generation of mineral growth in the MSU, represented by hypidioblastic, Ca-poor garnet cores and hypidioblastic, inclusion-rich staurolite is attributed to the Permian metamorphic event (e.g. Schuster *et al.*, 2001; Thöni & Miller, 2009). The second generation consisting of Ca-rich garnet + staurolite + chloritoid + chlorite + muscovite + paragonite as well as the conspicuous chloritoid pseudomorphs is attributed to the Eoalpine event (as described in the Plankogel Unit in the Koralpe by Gregurek *et al.* (1997). The same high-*P*–low-*T* metamorphic event overprinted the metapelites in the EGU, whereby possible Permian relicts have been largely erased and embedded basic rocks were transformed into eclogites (e.g. Miller & Thöni, 1997). The widespread fine-grained kyanite aggregates (paramorphs after Permian andalusite) as well as relict low-*P*–high-*T* assemblages indicate a Permian precursor history of the EGU (e.g. Habler & Thöni, 2001).

CONVENTIONAL THERMOBAROMETRY

In order to test if the formation conditions of the different assemblages in the foot- and hangingwall of the Plankogel detachment fulfil the criteria predicted by an extraction fault mechanism, we begin with determining the metamorphic field gradient across the southern Saualpe area. To constrain the peak high-*P* conditions achieved by the EGU during the Eoalpine event, a representative sample of metabasic eclogite was chosen. Three samples of garnet–biotite–staurolite–kyanite micaschists of the EGU in the footwall have been investigated to define the metamorphic conditions of the decompressed high-grade metapelites. Several specimen of the MSU of the hangingwall have been analysed to infer whether conditions change as a function of the distance from the Plankogel detachment. *P–T* determinations (inverse modelling) for metapelites used THERMOCALC v.3.37 and the average *P–T* method (*av*PT) of Powell & Holland (1994). The end-member activities were determined from chemical analysis data using the software AX (http://www.esc.cam.ac.uk/research/research-groups/research-projects/tim-hollands-software-pages/ax).

Chlorite was excluded from calculations for the EGU as it is considered to be of late retrograde origin. Microstructural relationships suggest chlorite in the MSU forms part of the equilibrium assemblage. Water was assumed to be in excess as all investigated samples are rich in hydrous equilibrium phases. Independent reactions used for *P–T* determinations are shown in Tables 5 and 6. Results are reported in Table 7. Some calculations for samples of the MSU are affected by high uncertainties for the pressure determination (e.g. sample GGP6 & GGP2). These rocks lack petrologically useful phases (kyanite, plagioclase and biotite), which limits conventional thermobarometry and causes large errors. Some calculations yield conspicuously high temperatures attributed to variable H_2O-saturation, which has been documented for both the Sau- and Koralpe (Tenczer *et al.*, 2006).

In order to estimate the *P–T* relations of the metabasic eclogites, an exchange geobarometer and -thermometer was used respectively. The kyanite and quartz absent reaction diopside + muscovite = grossular + pyrope + celadonite calibrated by Krogh Ravna & Terry (2004) was used for pressure calculations. Temperature was determined by using a garnet–clinopyroxene Fe^{2+}–Mg geothermometer (Krogh Ravna, 2000). The calculations were carried out using the spreadsheet of Krogh Ravna & Terry (2004), whereas pressure and temperature are computed by iteration. Hence, the equilibrium *P–T* is given by the intersection of the two equilibria in *P–T* space. Since only one of the investigated eclogite specimens bears phengite (sample B1), calculations were carried out using measurements of this sample only (Table 5). The eclogite sample records average peak conditions computed from mineral rim-compositions of ~23–24 kbar and 640–690 °C (see employed

measurements and results in Table 5). The equilibrium used for pressure calculation has average standard deviations of ±3.2 kbar (Krogh Ravna & Terry, 2004). The exchange thermometer is affected by uncertainties of ±60 °C due to poor constraints on the content of ferric iron (Krogh Ravna & Paquin, 2004). The calculated values are consistent with findings of Thöni *et al*. (2008).

Results are plotted along the field transect (dotted line in Fig. 1c) and displayed in Fig. 5, illustrating the lack of a gradient in equilibrium pressures, except for the metabasic eclogites. All sampled metapelites are equilibrated to roughly the same conditions, irrespective of their structural location in the foot- or hangingwall of the Plankogel detachment. This suggests that all units equilibrated at a comparable crustal level, with exception of eclogites on the northern end of the transect. Due to their chemical composition, eclogites are in general more sluggish with respect to equilibration when compared to metapelites. Hence, the metabasites are interpreted to record the Eoalpine peak pressure conditions (e.g. Thöni *et al*., 2008), while the metapelites equilibrated at a later stage during the exhumation history.

PHASE EQUILIBRIUM MODELLING

While the metabasic eclogites are ideal to infer conditions at the metamorphic peak and hence the depth of burial of the EGU in the footwall, peak pressure conditions for the MSU in the hangingwall cannot be determined directly by conventional thermobarometry. This is due to the possibility that equilibrium has been achieved along the retrograde exhumation path, and hence at lower conditions than the Eoalpine metamorphic peak. Forward thermodynamic modelling can bypass this problem and be used to infer peak conditions from microstructural relationships since the mineral assemblage itself is less prone to changes in the physical conditions than the chemical composition of the respective phases. In order to constrain the complex metamorphic history of the southern Saualpe area, pseudosections have therefore been constructed for characteristic rocks from either side of the Plankogel detachment: (i) for the MSU in the hangingwall of the detachment, sample GGP6 has been chosen because of its conspicuous chloritoid pseudomorphs which have the potential to provide tight constraints on the metamorphic evolution. (ii) For the EGU in the footwall of the Plankogel detachment, a representative sample of a decompressed metapelites (sample A33) was chosen to reconstruct the eclogite facies Eoalpine evolution.

Model parameters

Pseudosections were calculated using THERMOCALC v.3.37 with the internally consistent thermodynamic data set ds6 (Holland & Powell, 2011). Modelling was carried out in the 11-component system $MnO–Na_2O–CaO–K_2O–FeO–MgO–Al_2O_3–SiO_2–H_2O–TiO_2–O$ (MnNCKFMASHTO) considering the following solid solution models: garnet, staurolite, chloritoid, chlorite, paragonite, margarite, epidote, magnetite, ilmenite, hematite, plagioclase, K-feldspar and melt (White *et al*., 2000, 2014a,b; Holland & Powell, 2003). Pure phases include andalusite, kyanite, sillimanite, titanite, rutile, lawsonite, quartz and H_2O.

The content of ferric iron was estimated following Diener & Powell (2010) by the construction of several *T–X* and *P–X* pseudosections with variable amounts of ferric iron. Except for the oxide phases and epidote, which contain significant amounts of ferric iron, the silicate stability fields were only moderately affected by the effective amount of Fe^{3+}, save for unrealistic high contents. A robust assumption of Fe^{3+} was then assumed and is listed in Table 8.

H_2O was assumed to be in excess when modelling the MSU. The modelled rock is rich in hydrous phases such as chloritoid and white mica (50–60% in modal proportions, Fig. 2e,f). No evidence of melting that might have dehydrated the rocks has been observed. Furthermore, water saturation is supported by the enormous time gap that lies between the two events affecting the area: the Permian event reached its peak conditions *c*. 270 Ma; the rocks then cooled until *c*. 190 Ma without being exhumed (Schuster *et al*., 2001). The Eoalpine event, however, experienced its peak at *c*. 92 Ma (Thöni *et al*., 2008). This implies that *c*. 90–100 Ma lie between the two events and (local) re-hydration followed by fixing some free water in hydrous low-grade minerals such as sericite or chlorite is likely. These phases suggest that abundant water was available for metamorphic reactions during the prograde Eoalpine evolution. In contrast, the metapelitic gneisses of the footwall (EGU) feature a *P–T* path that is known to lie partly within or at

Table 5. End-member reactions, calibrations and results for *P–T* determinations for metabasic eclogite using exchange thermobarometers.

Sample	Assemblage	Reactions	Calibration	*P* (kbar)	SD (kbar)	*T* (°C)	SD (°C)
B1	3grt, 18omph, 13wm	di + ms = grs + prp + cel	Krogh Ravna & Terry (2004)	23	3.2	–	–
		alm + di = prp + hd	Krogh Ravna (2000)	–	–	650	60
B1	7grt, 19omph, 13wm	di + ms = grs + prp + cel	Krogh Ravna & Terry (2004)	24	3.2	–	–
		alm + di = prp + hd	Krogh Ravna (2000)	–	–	690	60
B1	3grt, 17omph, 16wm	di + ms = grs + prp + cel	Krogh Ravna & Terry (2004)	23	3.2	–	–
		alm + di = prp + hd	Krogh Ravna (2000)	–	–	640	60

Table 6. End-member reactions used for thermobarometric calculations on metapelites using THERMOCALC. The phases in brackets have been assumed in excess. Mineral abbreviations are those used in the software.

Sample	Assemblage	Reactions	
A33	grt + bi + st + pl + ms (+ q + ky + H_2O)	gr + q + ky = an	phl + east + q = py + cel
		gr + mst + q = py + an + H_2O	phl + ky = py + east + q
		gr + fst + q = alm + an + H_2O	ann + mu + q = alm + fcel
		gr + pa + q = an + ab + H_2O	ann + q + ky = alm + mu
		east + q = py + phl + mu	
A6	grt + bi + st + pl + ms (+ q + ky + H_2O)	gr + q + ky = an	phl + east + q = py + cel
		gr + mst + q = py + an + H_2O	phl + ky = py + east + q
		gr + fst + q = alm + an + H_2O	ann + mu + q = alm + fcel
		gr + pa + q = an + ab + H_2O	ann + fst + q = alm + mu + H_2O
		east + q = py + phl + mu	
A11	grt + bi + st + pl + ms (+ q + ky + H_2O)	gr + q + ky = an	ann + mu + q = alm + fcel
		gr + mst + q = py + an + H_2O	ann + q + ky = alm + mu
		gr + fst + q = alm + an + H_2O	east + q = phl + py + mu
		gr + pa + q = an + ab + H_2O	phl + ky = east + py + q
		phl + east + q = py + cel	
A29	grt + st + ms + chl (+ q + H_2O)	py + daph + ames + q = clin + fst	alm + mu + daph + q = fcel + fst
		cel + ames = mu + clin	fcel + fst = alm + mu + q + H_2O
		py + mu + clin + q = cel + mst	py + alm + mu + clin + q = cel + fst
A8	grt + st + cld + ms + chl (+ q + H_2O)	clin + mst = py + mctd + ames	fctd + q = daph + fst + H_2O
		clin + mst + q = py + mctd	py + fctd = alm + mctd
		py + mctd = clin + mst + H_2O	daph + fcel + fst = alm + fctd + mu
		alm + fctd = daph + fst + H_2O	clin + cel + mst = py + mctd + mu
C3	grt + bi + st + pl + ms (+ q + ky + H_2O)	east + q = py + phl + mu	ann + mu + q = alm + fcel
		phl + mst = py + east + mu + H_2O	ann + fcel + fst = alm + mu + H_2O
		phl + east + q = py + cel	py + east + fcel = alm + phl + mu
		phl + ky = py + east + cel	
C14	grt + bi + st + ms + chl (+ q + H_2O)	py + mu + clin + q = cel + mst	alm + daph + ru = ilm + fst + q
		py + mu + ames + q = cel + mst	py + alm + mu + clin + q = cel + fst
		alm + mu + daph + q = fcel + fst	alm + cel + ru = py + mu + ilm + q
		fcel + fst = alm + mu + q + H_2O	
A20	grt + bi + st + pl + ms (+ q + ky + H_2O)	gr + q + ky = an	mst + phl = py + east + q + H_2O
		gr + mst + q = py + an + H_2O	east + q = py + mu + cel
		gr + fst + q = alm + an + H_2O	ann + mu + q = alm + fcel
		gr + pa + q = an + ab + H_2O	fst + ann + q = alm + mu + H_2O
		east + q = py + phl + mu	
GGP6	grt + st + cld + ms + chl (+ q + H_2O)	clin + mst = ames + mctd + py	fctd + alm = daph + fst + H_2O
		ames + py + q = clin + mctd	clin + fst = daph + ames + mctd + py
		mctd + py = clin + mst + H_2O	clin + daph + fst = ames + mctd + alm
GGP2	grt + st + cld + ms + chl (+ q + H_2O)	py + mctd + ames = mst + clin	py + fst = alm + mst
		mst + clin + q = py + mctd	py + fctd = alm + mctd
		py + mctd = mst + clin + H_2O	cel + mst + clin = py + mctd + mu
		fst + daph + q = alm + fctd	py + fcel = alm + cel

Table 7. Results of *P–T* calculations for metapelite samples from footwall (EGU) and hangingwall (MSU). Values are graphically illustrated in Fig. 5.

Sample	Unit	*P* (kbar)	SD (kbar)	*T* (°C)	SD (°C)
A33	EGU	9.8	1.0	655	16
A6	EGU	8.6	1.2	685	23
A11	EGU	9.4	2.5	716	52
A29	MSU	12.8	2.8	579	25
A8	MSU	11.6	1.5	578	8
C3	MSU	10.1	1.5	620	26
C14	MSU	8.6	1.4	605	14
A20	MSU	8.8	1.3	697	20
GGP6	MSU	10.4	2.4	583	11
GGP2	MSU	9.4	1.7	575	8

least near the partial melting field (e.g. Tenczer *et al.*, 2006; Eberlei *et al.*, 2014). As the melt proportion highly depends on the water content, but little evidence of large amounts of melt are known in these rocks, we assume an amount of H_2O that guarantees a wet solidus (following the logic of Zeh *et al.*, 2004). As such, in the pseudosection for sample A33 (Fig. 6b) the suprasolidus part of the diagram is calculated with 2.2 wt% H_2O. The subsolidus part is assumed to be saturated in H_2O (Table 8).

Determination of the effective bulk composition

Thermodynamic modelling requires bulk compositions to be determined. The Permian metamorphic event was the first pervasive metamorphism that affected the

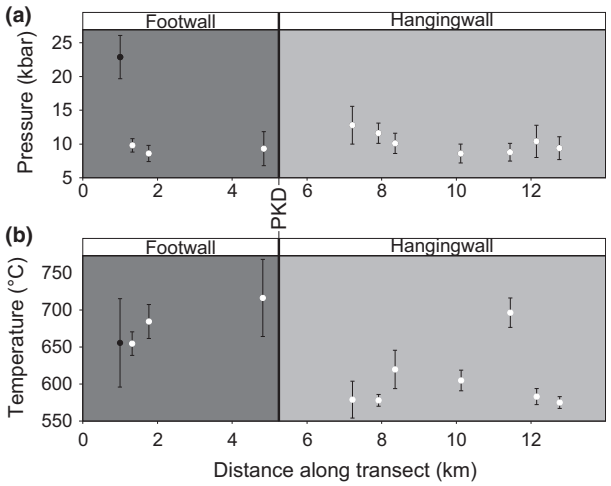

Fig. 5. Metamorphic field gradients of the southern Saualpe transect shown in Fig. 1c. The black dots refer to the calculations for the eclogite sample B1 (Table 5) while the white dots correspond to data for metapelites (Table 7). Error bars are for 1σ. PKD stands for Plankogel detachment (a) Plot of the variations in equilibrium pressure. (b) The corresponding variations in temperature.

area of interest causing complete equilibration at the metamorphic peak (Tenczer *et al.*, 2006). During the Eoalpine metamorphism, however, only incomplete equilibration was achieved as indicated by complexly zoned garnet of the MSU in the hangingwall (e.g. sample GGP6, Fig. 4b,d). This indicates isolation of reactants in garnet cores, which show evidence for multistage-growth under changing *P–T* conditions (Fig. 3b,d). Incomplete equilibration between two metamorphic events implies different effective bulk compositions for the two events (e.g. Stüwe, 1997; Tenczer *et al.*, 2006). In order to estimate the effective bulk composition for the later, incompletely equilibrated event from the whole-rock analysis, the approach of Evans (2004) was used. This method is based on the correlation between the amount of MnO sequestered in garnet cores and the modal proportion of garnet, which is expressed through Rayleigh fractionation. A simplification is given by the assumption that garnet is the only Mn-bearing phase; other Mn-incorporating phases (e.g. staurolite, chlorite and chloritoid) have been neglected. By plotting the calculated garnet mode *v.* the trend of major elements (Ca, Fe and Mg), the amount of sequestered elements can be determined. An integration of the respective profiles between the zero amount of the earliest-grown garnet (i.e. the most spessartine-rich core) and the modal amount of garnet at a point of interest is used. The amount of incorporated SiO_2 and Al_2O_3 is linked to the other garnet-forming elements by stoichiometry. The entire Permian garnet core was subtracted as illustrated in Fig. 4d.

Since strong discontinuous garnet zoning is lacking in metapelites from the EGU in the footwall, complete equilibration during the Eoalpine event is assumed. A bulk correction has therefore been neglected and the XRF-derived bulk composition was used for pseudosection modelling. The measured Permian- and the calculated Eoalpine bulk compositions of sample GGP6 and A33, respectively, are shown in Table 8.

EOALPINE PSEUDOSECTIONS

In order to infer the metamorphic evolution for the units in the foot- and hangingwall of the Plankogel detachment, a separate discussion of pseudosections for the footwall and the hangingwall follows.

P–T evolution of the hangingwall (MSU, sample GGP6)

The prograde Eoalpine evolution of the hangingwall can be interpreted from thermodynamic modelling and major element zoning pattern in garnet from the MSU (Figs 2f & 4b). Garnet isopleth modelling (solid blue lines in Fig. 6a) predicts a grossular-rich first stable garnet. Hence, the grossular-rich rim (X_{Grs} = 0.14–0.16; Fig. 4b,d) corresponds to the onset of garnet stability, i.e. the occurrence of the first Eoalpine garnet. This yields the starting point of the *P–T* path (shaded arrow in Fig. 6a), which crosses the garnet-in line ~10–12 kbar and 500–550 °C, corresponding to the maximum grossular-content in the garnet profile of sample GGP6 (Fig. 4d). The modelled grossular-content decreases significantly from a maximum of ~0.14 to ~0.04 with increasing pressure and temperature. This striking change in grossular-content is consistent with the chemical profile illustrated in Fig. 4d. Although the X_{Grs} displays a large drop, the modelled garnet growth only reaches ~5% in modal amount along the prograde path (black dashed lines in Fig. 6a). This limited garnet growth is consistent with the thin Eoalpine rim observed (Figs 2f & 4d).

The suggested *P–T* path is illustrated as a shaded arrow in Fig. 6a. The end point is determined by the results of thermobarometry based on the final assumed

Table 8. Bulk rock compositions in mol.% used for phase diagram modelling.

Sample	Comment	MnO	Na_2O	CaO	K_2O	FeO	MgO	Al_2O_3	SiO_2	TiO_2	O	H_2O
GGP6	Permian bulk	0.32	1.60	0.25	3.63	12.24	3.57	24.06	52.35	1.38	0.59	Excess
GGP6	Eoalpine bulk	0.10	1.78	0.16	4.02	10.94	2.36	25.12	53.39	1.53	0.63	Excess
A33	Subsolidus	0.14	1.54	0.90	2.71	7.47	3.69	15.08	67.24	0.89	0.36	Excess
A33	Suprasolidus	0.13	1.41	0.82	2.49	6.86	3.39	13.86	61.80	0.81	0.33	8.09

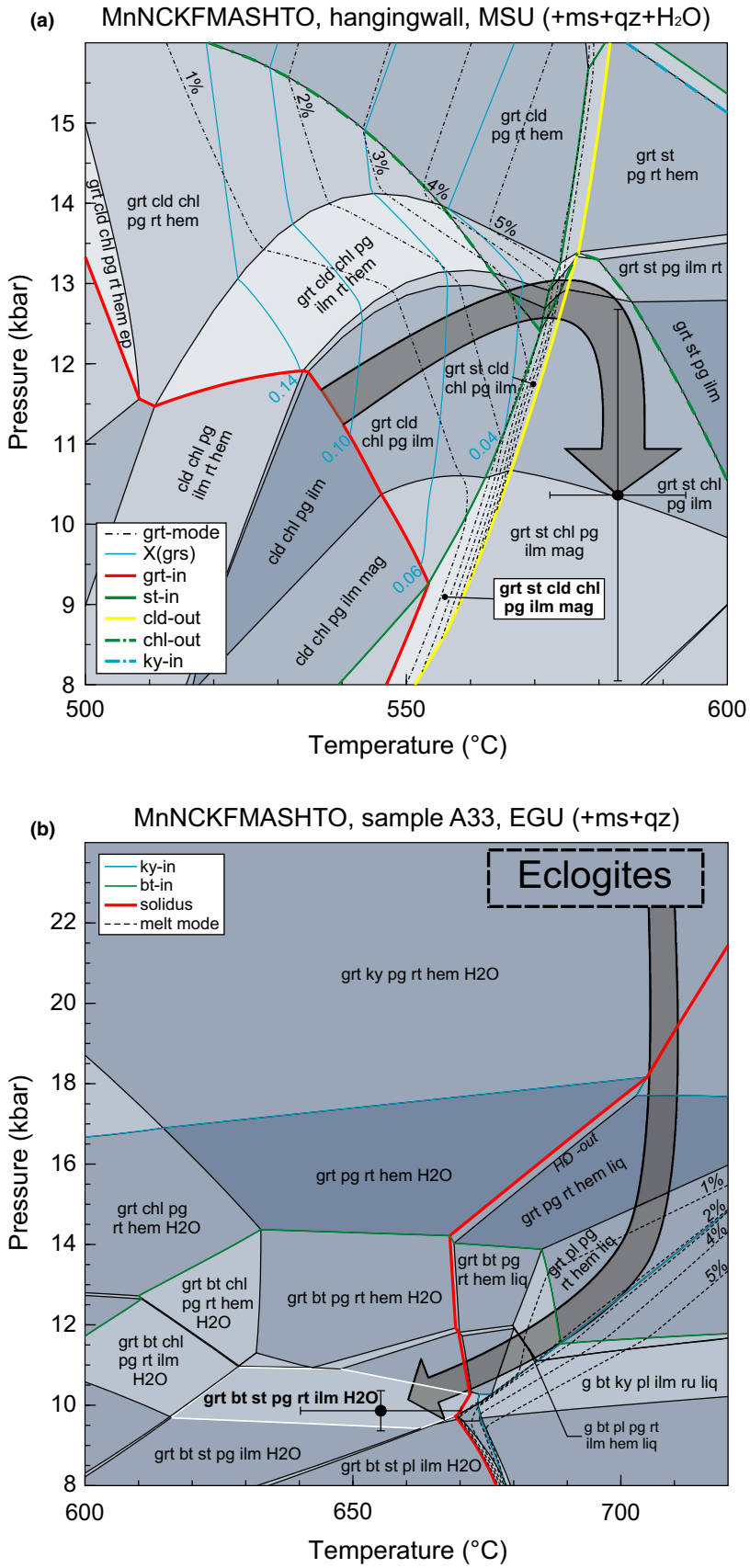

Fig. 6. *P–T* pseudosections for two samples from the foot- and hangingwall of the Plankogel detachment respectively. *P–T* cross from conventional thermobarometry. Shaded arrows indicate the proposed *P–T* path. The shading of the stability fields indicates the variance of the respective field. The darker colour indicates higher variance. Phases in brackets are assumed in excess. The employed bulk compositions are reported in Table 8. (a) MnNCKFMASHTO pseudosection for the hangingwall (MSU, sample GGP6) with the inferred equilibrium assemblage (bold). The solid blue lines are grossular-isopleths. (b) MnNCKFMASHTO pseudosection for the footwall (EGU, sample A33) with the inferred equilibrium assemblage (bold). The subsolidus part is assumed to have H_2O in excess; the suprasolidus part is calculated with 2.2 wt% H_2O. The dashed lines correspond to melt modes.

equilibrium assemblage (cross in Fig. 6a; Table 7). Straight grain boundaries indicate equilibrium coexistence of chloritoid and staurolite (Fig. 2h), as predicted by pseudosection modelling (see the narrow trivariant grt + st + cld + chl + pg + ilm + mag field in Fig. 6a, delimited by the solid green and yellow lines). Following this, the maximum estimated temperature experienced by these units is in the range of 550–580 °C. Conventional *P–T* determinations indicate that equilibrium was achieved close to the mentioned field (cross in Fig. 6a). The presumed peak pressure conditions for the MSU are estimated to have not exceeded 12–14 kbar since the rocks are interpreted to have never left the chlorite stability field (dashed green line in Fig. 6a). Additionally, at higher pressures the appearance of kyanite is predicted (dashed blue line in Fig. 6a). However, no trace has been observed in this sample. Therefore, we infer a maximum pressure experienced by the hangingwall of the Plankogel detachment bound to the stability field of chlorite and inferior to the stability of kyanite.

P–T evolution of the footwall (EGU, sample A33)

For the EGU in the footwall of the Plankogel detachment, the metabasic eclogite boudins scattered in volumetrically dominant metapelites indicate that the entire pile has experienced the same high-*P*–low-*T* Eoalpine metamorphic evolution. This assumption is corroborated by recrystallization ages of garnet, staurolite and white mica from the metapelitic host-rocks defined by concordant Sm/Nd and Rb/Sr isochrons of *c.* 90 ± 3 Ma, being virtually identical to the timing of the Eoalpine peak recorded in eclogites (Thöni & Jagoutz, 1992). Calculated peak conditions from eclogite B1 provide the starting point for the retrograde evolution of the decompressed metapelites with the representative sample A33 (Fig. 6b). Based on microstructural relationships and conventional thermobarometry, a *P–T* path can be determined, as illustrated by the shaded arrow in Fig. 6b: kyanite inclusions in biotite indicate that the alumosilicate formed prior to biotite, thus kyanite is assumed to have been stable during the entire exhumation history. Hence, the *P–T* path is thought to plot close to the kyanite stability field and results to be largely isothermal in the early stages of exhumation. The modelled peak assemblage consisting of garnet + kyanite + paragonite + rutile + hematite (+ muscovite + quartz + H_2O) is interpreted to have experienced a small degree of melting along the decompression path (a modelled maximum of ~3% in mode) as consistent with the literature (e.g. Tenczer *et al.*, 2006; Eberlei *et al.*, 2014). Similar to kyanite, plagioclase is predicted as a metastable phase in the thin-section assemblage. Garnet inclusions in hypidioblastic staurolite suggest that the latter grows along the late retrograde path as predicted by the model.

DISCUSSION

Before discussing the Eoalpine evolution of the foot- and hangingwall of the Plankogel detachment in a geodynamic context, our interpretations are briefly reported for the formation of the chloritoid pseudomorphs present in sample GGP6 from the MSU.

Eoalpine chloritoid pseudomorphs

Pseudosection modelling can be used to constrain the formation of the chloritoid pseudomorphs (sample GGP6, Fig. 2e,g). Regarding the polymetamorphic nature of the area, the precursor phase could have grown during the Permian high-*T*–low-*P* event. We tentatively suggest that coarse-grained Permian staurolite is a likely phase for pseudomorphic replacement by Eoalpine chloritoid: thermodynamic modelling predicts a nearly isothermal staurolite-in line starting at ~540 °C and 8 kbar (solid green line in Fig. 6a). This indicates that any (Permian) staurolite is unstable at temperatures below this stability line during the prograde Eoalpine metamorphism. Chloritoid, however, is modelled to be stable at temperatures below 550–580 °C (indicated by the solid yellow line in Fig. 6a). Thus, large Permian staurolite which survived retrograde consumption or alteration is thought to have been replaced by chloritoid along the prograde Eoalpine *P–T* path (shaded arrow in Fig. 6a). The prismatic morphology of the pseudomorphs supports this assumption. The replacement of precursor Permian staurolite by Eoalpine chloritoid could occur along the prograde *P–T* path in the staurolite-absent field (shaded arrow in Fig. 6a). Furthermore, the high alumina content in staurolite with respect to chloritoid (~50 wt% *v.* ~40 wt%, respectively, Table 4) indicates liberation of excessive alumina during the replacement which resulted in formation of the fine-grained sericite and paragonite present inside the pseudomorphs. A fluid-driven process is suspected to induce the local pseudomorphic replacement. As soon as the *P–T* path crossed the staurolite-in line (solid green line in Fig. 6a) the crystallization of Eoalpine staurolite (st II) commenced. The latter is present commonly as rock-forming mineral in the matrix (st II; see petrography section).

Eoalpine evolution of footwall and hangingwall

In summary, forward pseudosection and inverse *P–T* modelling on selected samples from both sides of the Plankogel detachment in the southern Saualpe have shown that: (i) the EGU in the footwall experienced Eoalpine eclogite facies metamorphism with peak conditions of 22 ± 2 kbar and 630–740 °C (Thöni *et al.*, 2008). *P–T* determinations on eclogite nodules are consistent with these results. (ii) Based on pseudosection modelling, the MSU in the hangingwall reached peak conditions of ~12–14 kbar and 550–580 °C. Fur-

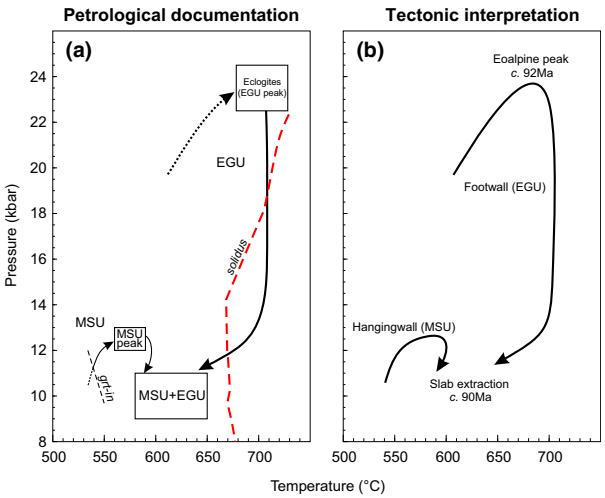

Fig. 7. Simplified *P–T* path showing the postulated evolution during the Eoalpine event for the Eclogite Gneiss Unit and the Micaschist Unit in the foot- and hangingwall of the Plankogel detachment respectively. (a) Petrological evolution. The starting point for the prograde path of the Micaschist Unit is given by the garnet-in line modelled for sample GGP6 (Fig. 6a). The dashed red line represents the wet solidus modelled for sample A33 (Fig.6b) and is interpreted as representative for the metapelites in the Eclogite Gneiss Unit. (b) Interpreted tectonic evolution of the foot- and hangingwall in a temporal frame.

thermore, the complete absence of eclogites or retrogressed high-*P* assemblages in both the MSU in the Saualpe and the Plankogel Unit in the Koralpe argue strongly against a high-*P* evolution for the hangingwall of the Plankogel detachment (Gregurek *et al.*, 1997). (iii) The rocks in the foot- and the hangingwall were exhumed by different extent to similar mid crustal levels where assemblages equilibrated at similar conditions of ~10 kbar and 580–650 °C. The proposed *P–T* evolution for the foot- and the hangingwall of the detachment (Fig. 7) is consistent with evidence from the Koralpe further to the east: Gregurek *et al.* (1997) documented that the rocks of the Koralpe Complex in the footwall of the Plankogel detachment equilibrated at eclogite facies conditions while pressures recorded in the Plankogel Unit in the hangingwall did not exceed 10–11 kbar. These authors also suggested that the units in the foot- and hangingwall resided at different depths during early Eoalpine metamorphism and both units joined one *P–T* path later in their evolution (see fig. 7 in Gregurek *et al.*, 1997). Therefore, it is meaningful to interpret the Plankogel detachment across the Saualpe and the Koralpe as a single major detachment, whereas both regions experienced a similar exhumation history.

Implications for the exhumation model

In the Saualpe, the difference between the peak pressures experienced by the footwall and the pressure where foot- and hangingwall equilibrated together is in the order of ~10–12 kbar, with a somewhat smaller magnitude in the Koralpe (Gregurek *et al.*, 1997). This corresponds to a vertical thickness of ~37–44 km, assuming a crustal density of 2750 kg m^{-3} (neglecting tectonic overpressure). As both units experienced roughly the same degree of retrograde equilibration at comparable depth, a two-stage exhumation mechanism is suggested: first, both foot- and hangingwall were brought to a similar crustal level followed by a second, later stage involving final exhumation to the surface. The mechanism preferred here is that of slab extraction as proposed by Froitzheim *et al.* (2003). We further suggest that both the Plankogel detachment and the PGSZ are part of the same extraction fault system (see Fig. 1d and Kurz *et al.*, 2002). We suggest that, during early Eoalpine subduction, a major lithospheric slab was extracted along the trace of the Plankogel suture as well as within the PGSZ and extracted downwards (southwards) (Fig. 8). In this model, exhumation is driven by the negative buoyancy of the extracted slab and not by positive buoyancy of the subducted continental crust (Janák *et al.*, 2006).

During the process, rocks near the upper limiting point of this slab (black and white diamonds in Fig. 8) converged only by few kilometres. This corresponds to the PGSZ of the Koralpe, for which Eberlei *et al.* (2014) have inferred a channel flow process – consistent with our interpretation. Rocks further down along the block converged increasingly more (black and white dots in Fig. 8). This coincides with the foot- and hangingwall of the Plankogel detachment, respectively, and matches the pressure difference documented here. Once the entire slab was extracted, exhumation was intermittently terminated, giving the rocks some time to equilibrate at mid crustal levels. This was followed by a second stage involving the ascent of the units to the surface, probably as a result of extensional and erosional exhumation (Froitzheim *et al.*, 2003; Janák *et al.*, 2004). A comparable model for the exhumation of UHP units in the Pohorje Massif was described by Janák *et al.* (2004, 2006, 2015). These authors propose the downward extraction of substratum belonging to the Upper Central Austroalpine. The process may have been facilitated by the negative buoyancy of dense material (part of the Meliata-Hallstatt oceanic domain) attached to the slab (Janák *et al.*, 2004, 2015).

Structural predictions

The downward extraction of a prominent slab of several tens of kilometres in thickness has an important structural implication: it predicts that the extraction fault that was formed in the process is characterized by opposing shear senses in the foot- and hangingwall of the extracted slab. Considering that the PGSZ

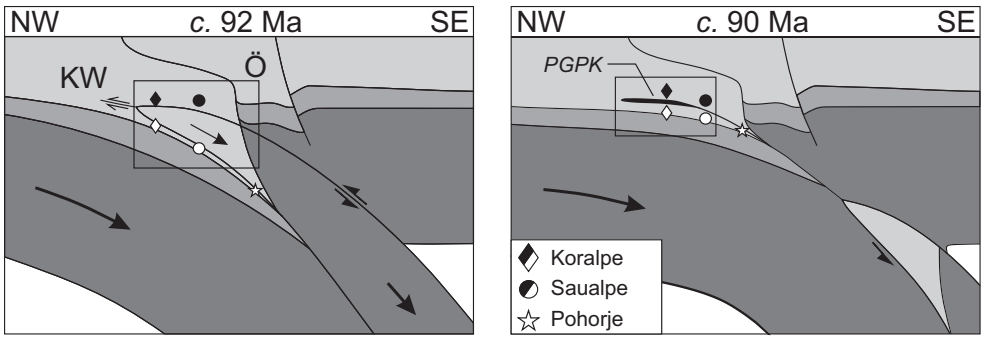

Fig. 8. Simplified tectonic sketch showing the Eastern Alps during the Eoalpine subduction illustrating the interpretation of the Plattengneiss-Plankogel shear system (PGPK) as suggested here. The dots demark the supposed positions for the Eclogite Gneiss Unit (white dots) and the Micaschist Unit (black dots) from the foot- and hangingwall of the Plankogel detachment respectively. The diamonds indicate the locations for units in the footwall (white diamonds) and the hangingwall (black diamonds) of the Plattengneiss shear zone of the Koralpe. The white star corresponds to the approximate location of the Pohorje UHP units (Janák *et al.*, 2004, 2006, 2015). The box in the left-hand cross-section indicates the supposed location of the Saualpe–Koralpe area inside the Koralpe-Wölz Complex (KW) before slab extraction. Ö = Ötztal Complex. The right-hand sketch displays the interpreted situation during onset of rapid isostatic uplift shortly after slab extraction which brings the units in contact (Froitzheim *et al.*, 2003) following a largely isothermal decompression path.

of the Koralpe and the Plankogel detachment of both the Koralpe and the Saualpe are part of the same shear zone system (Fig. 1d), this model yields the following predictions: for the Plattengneiss, the south-directed flow of material is responsible for strong syn-deformational flattening of the shear zone as inferred by Eberlei *et al.* (2014). A pressure gap of up to 3 kbar across the PGSZ reported by these authors is consistent with a loss of material from within the shear zone. A spatial reversal of shear sense within the shear zone has also been suggested by Eberlei *et al.* (2014) and was previously implicitly documented by Kurz *et al.* (2002).

As such, the PGSZ of the Koralpe may be interpreted as the upward (and northward) termination of the extraction fault (Fig. 8). In the Saualpe, rocks expose slightly lower crustal levels, so that the equivalent of the Plattengneiss might has been eroded there. Regrettably, shear sense in the Plankogel detachment is not easily determined, in part due to bad outcrop conditions. Nevertheless, ambiguous shear sense indicators indicating both top-to-the-north and top-to-the-south shear sense have been reported in the literature (Pilger & Schönenberg, 1975). In this sense the model of slab extraction provides an explanation for the ambiguous nature of the shear sense indicators in the entire region and is consistent with the Plankogel detachment being the downward (and southward) continuation of the extraction fault. In fact, as the downwardly extracted slab widens with depth, a more distributed deformation is expected at depth. This is consistent with the Plattengneiss being a mylonitic horizon and the Plankogel detachment being somewhat less deformed with more distributed deformation.

Other models that have been suggested for the exhumation of the Kor- and Saualpe include the model of Kurz *et al.* (2002) and that of Wiesinger *et al.* (2006). The model of Kurz *et al.* (2002) is not unlike the exhumation of core complexes and is based on data indicating that shear sense in the PGSZ might be top-to-the-north in the north and top-to-the-south in the south. However, this model was suggested before the geometry of the PGSZ was known (Putz *et al.*, 2006) and the data of Kurz *et al.* (2002) may also be interpreted in terms of top-to-the-north shear sense in the footwall of the shear zone and top-to-the-south shear sense in the hangingwall (Eberlei *et al.*, 2014). Therefore, the model of Kurz *et al.* (2002) is subsumed by the slab extraction model proposed here. Conversely, the model of Wiesinger *et al.* (2006) interprets the Plankogel detachment in terms of a Chemenda-type extrusion wedge (Chemenda *et al.*, 1995, 1996). Wiesinger *et al.* (2006) suggested that the EGU was extruded up- and northwards from underneath the MSU. This model is inconsistent with the two-stage exhumation for which we show evidence here. According to Janák *et al.* (2006), this scenario is also unlikely because of the lack of sedimentary record indicating erosion of large volumes of rocks having a Cretaceous metamorphic fingerprint (Von Eynatten & Gaupp, 1999). In summary, we suggest that the model of a downwards extracting slab is the scenario that is most consistent with the petrologically documented two-phase exhumation and the reported shear sense indicators.

One of the major remaining problems of the model presented here is that it predicts that the hangingwall rocks of the PGSZ in the Koralpe should be similar to those of the MSU in the hangingwall of the Plankogel detachment in the Saualpe. While we have no unique solution for this problem, it is suggested that this may be explained through the three-dimensional nature of the process and emphasize that our model is schematic.

Temporal relations

Geochronolgical data from the literature allow tight timing constraints on the various stages of the process inferred here (Fig. 7b). Indeed, they are consistent with and supportive of the model presented here. (i) The Eoalpine pressure peak in the Saualpe area was reached at *c*. 91 ± 3 Ma (Thöni *et al*., 2008). As the rocks were buried and heated until the slab extraction process started, this time is probably related to the onset of downward motion of the isolated body. (ii) The extraction of the slab was completed after a rather short time span. Froitzheim *et al*. (2003) attributed no more than 2 Ma for this process. Accordingly, Thöni (2006) suggested that eclogites from the Koralpe were exhumed from high-*P* conditions to depths of less than 20 km in *c*. 3–7 Ma. Rapid exhumation is consistent with an initially isothermal exhumation path for which we show evidence here (Fig. 6b). (iii) Wiesinger *et al*. (2006) documented that the EGU reached the closure temperature of $^{39}Ar/^{40}Ar$ in white mica between 85.6 and 78.1 Ma during exhumation. This may be the time of the onset of the second stage of exhumation following equilibration of footwall and hangingwall at mid crustal levels. (iv) Final exhumation of the Saualpe–Koralpe block to the surface is documented by apatite fission track ages between 52 and 31 Ma (Wölfler *et al*., 2011). $^{39}Ar/^{40}Ar$ crystallization ages of white mica from the PU range from 130 to 123 Ma, which is representative for the timing of Eoalpine nappe stacking (Wiesinger *et al*., 2006). Therefore, the ages determined for the PU predate Eoalpine peak conditions recorded in the EGU (e.g. Thöni *et al*., 2008), implying that the low-grade units are not part of the subduction-related eclogite facies metamorphism (Wiesinger *et al*., 2006).

CONCLUSIONS

The Plankogel detachment of the Eastern Alps bounds the Cretaceous high-*P* rocks of the eclogite type locality in the Saualpe–Koralpe area to the south. Although it has long been recognized as a structure related to the exhumation of the high-grade rocks its tectonic significance has remained enigmatic. From our study, we now conclude the following:

(i) Eclogite facies rocks in the footwall of the Plankogel detachment in both the southern Saualpe and Koralpe formed at ~20 kbar and 680 °C with pressures in the Saualpe being marginally higher. Following peak pressures, the rocks evolved by nearly isothermal decompression to ~10 kbar.
(ii) Amphibolite facies rocks in the hangingwall of the detachment reached peak conditions of ~12–14 kbar and 550–580 °C. Both units joined and were subsequently exhumed together to a common crustal level leading to a common overprint at conditions of ~10 kbar and 580–650 °C.
(iii) We suggest that this evidence may be interpreted in terms of a slab extraction model in the sense of Froitzheim *et al*. (2003). The model for the Plankogel detachment matches earlier interpretations of the PGSZ as the loss of section and the opposite shear sense indicators at its top and bottom as suggested by Eberlei *et al*. (2014).
(iv) The Plankogel detachment forms the downward prolongation of the PGSZ along which syn-collisional exhumation of the Cretaceous high-*P* units occurred.

ACKNOWLEDGEMENTS

R. White and R. Palin are thanked for their comments and discussions. C. Hauzenberger and G. Hoinkes are thanked for their support and critical comments. R. Schuster made a critical review prior to submission of the final version of this manuscript. K. Ettingers assistance at SEM- and microprobe work is thankfully acknowledged. The manuscript was improved by thoughtful reviews of S. Raič. T. Johnson and two anonymous reviewers are thanked for their constructive comments.

REFERENCES

Becker, P., 1976. Gefügetektonische Studien an pegmatoiden Gneisen mit Plattengneistextur aus dem Gebiet östlich des Wölker Kogels (Stubalm, Steiermark). *Mitteilungen des Naturwissenschaftlichen Vereins für Steiermark*, **106,** 39–49.

Chemenda, A.I., Mattauer, M. & Bokun, A.N., 1995. Continental subduction and a mechanism for exhumation of high pressure metamorphic rocks: new modelling and field data from Oman. *Earth and Planetary Science Letters*, **143,** 173–182.

Chemenda, A.I., Mattauer, M., Malavieille, J. & Bokun, A.N., 1996. A mechanism for syn-collisional rock exhumation and associated normal faulting: results from physical modelling. *Earth and Planetary Science Letters*, **132,** 225–232.

Dachs, E., 1998. PET: petrological elementary tools for mathematica. *Computers & Geosciences*, **24,** 219–235.

Diener, J.F.A. & Powell, R., 2010. Influence of ferric iron on the stability of mineral assemblages. *Journal of Metamorphic Geology*, **28,** 599–613.

Eberlei, T., Johnson, T.E., White, R.W., Roffeis, C. & Stüwe, K., 2014. Thermobarometric constraints on pressure variations across the Plattengneiss shear zone of the Eastern Alps: implication for exhumation models during Eoalpine subduction. *Journal of Metamorphic Geology*, **32,** 227–244.

Evans, T.P., 2004. A method for calculating effective bulk composition modification due to crystal fractionation in garnet-bearing schist: implications for isopleth thermobarometry. *Journal of Metamorphic Geology*, **22,** 547–557.

Frank, W., 1987. Evolution of the Austroalpine elements in the Cretaceous. In: *Geodynamics of the Eastern Alps* (eds Flügel, H.W. & Faupl, P.), pp. 379–406. Deuticke, Vienna.

Fritsch, W., Meixner, H., Pilger, A. & Schönenberg, R., 1960. Die geologische Neuaufnahme des Saualpen-Kristallins (Kärnten) I. *Carinthia II*, **70–1,** 7–28.

Froitzheim, N., Pleuger, J., Roller, S. & Nagel, T.J., 2003. Exhumation of high- and ultrahigh pressure metamorphic rocks by slab extraction. *Geology*, **31,** 925–928.
Froitzheim, N., Pleuger, J. & Nagel, T.J., 2006. Extraction faults. *Journal of Structural Geology*, **28,** 1388–1395.
Froitzheim, N., Plašienka, D. & Schuster, R., 2008. Alpine tectonics of the Alps and Western Carpathians. In: *The Geology of Central Europe. Volume 2: Mesozoic and Cenozoic* (ed. McCann, T.), *Geological Society of London*, 1141–1232.
Gregurek, D., Abart, R. & Hoinkes, G., 1997. Contrasting P-T evolutions in the southern Koralpe, Eastern Alps. *Mineralogy and Petrology*, **60,** 61–80.
Habler, G. & Thöni, M., 2001. Preservation of Permo-Triassic low-pressure assemblages in the Cretaceous high-pressure metamorphic Saualpe crystalline basement (Eastern Alps, Austria). *Journal of Metamorphic Geology*, **19,** 679–697.
Haüy, M., 1822. *Traité de Minéralogie*, 2nd edn. Deuxième tome, Bachelier et Huzard, Paris.
Holland, T.J.B. & Powell, R., 2003. Activity–composition relations for phases in petrological calculations: an asymmetric multicomponent formulation. *Contributions to Mineralogy and Petrology*, **145,** 492–501.
Holland, T.J.B. & Powell, R., 2011. An improved and extended internally consistent thermodynamic dataset for phases of petrological interest, involving a new equation of state for solids. *Journal of Metamorphic Geology*, **29,** 333–383.
Janák, M., Froitzheim, N., Lupták, B., Vrabec, M. & Krogh Ravna, E.J., 2004. First evidence of ultrahigh-pressure metamorphism of eclogites in Pohorje, Slovenia: tracing deep continental subduction in the Eastern Alps. *Tectonics*, **23,** 1–10.
Janák, M., Froitzheim, N., Vrabec, M., Krogh Ravna, E.J. & De Hoog, J.C.M., 2006. Ultrahigh-pressure metamorphism and exhumation of garnet peridotite in Pohorje, Eastern Alps. *Journal of Metamorphic Geology*, **24,** 19–31.
Janák, M., Froitzheim, N., Yoshida, K. *et al*., 2015. Diamond in metasedimentary crustal rocks from Pohorje, Eastern Alps: a window to deep continental subduction. *Journal of Metamorphic Geology*, **33,** 495–512.
Krogh Ravna, E., 2000. The garnet–clinopyroxene Fe^{2+}–Mg geothermometer: an updated calibration. *Journal of Metamorphic Geology*, **18,** 211–219.
Krogh Ravna, E.J.K. & Paquin, J., 2004. Thermobarometric methodologies applicable to eclogites and garnet ultrabasites. *EMU Notes in Mineralogy*, **5,** 229–259.
Krogh Ravna, E.J. & Terry, M.P., 2004. Geothermobarometry of UHP and HP eclogites and schists – an evaluation of equilibria among garnet-clinipyroxene-kyanite-phengite-coesite/quartz. *Journal of Metamorphic Geology*, **22,** 579–592.
Kurz, W. & Fritz, H., 2003. Tectonometamorphic evolution of the Austroalpine Nappe Complex in the Central Eastern Alps consequences for the Eo-Alpine evolution of the Eastern Alps. *International Geology Review*, **45,** 1100–1127.
Kurz, W., Fritz, H., Tenczer, V. & Unzog, W., 2002. Tectonometamorphic evolution of the Koralm Complex (Eastern Alps): constraints from microstructures and textures of the Plattengneis shear zone. *Journal of Structural Geology*, **24,** 1957–1970.
Kurz, W., Wölfler, A., Rabitsch, R. & Genser, J., 2011. Polyphase movement on the Lavanttal fault zone (eastern Alps): reconciling the evidence from different geochronological indicators. *Swiss Journal of Geosciences*, **104,** 323–343.
Legrain, N., Stüwe, K. & Wölfler, A., 2014. Incised relict landscapes in the eastern Alps. *Geomorphology*, **221,** 124–138.
Massonne, H.J., 2012. Formation of amphibole and clinozoisite-epidote in eclogite owing to fluid infiltration during exhumation in a subduction channel. *Journal of Petrology*, 1–30.
Miller, C. & Thöni, M., 1997. Eoalpine eclogitisation of Permian MORB type gabbros in the Koralpe (Austria): new petrological, geochemical and geochronological data. *Chemical Geology*, **137,** 283–310.
Miller, C., Zanetti, A., Thöni, M. & Konzett, J., 2007. Eclogitisation of gabbroic rocks. Redistribution of trace elements and Zr in rutile thermometry in Eoalpine subduction zone (eastern Alps). *Chemical Geology*, **239,** 96–123.
Neugebauer, J., 1970. Alt-paläozoische Schichtfolge, Deckenbau und Metamorphose-Ablauf im südwestlichen Saualpen-Kristallin (Ostalpen). *Geotektonische Forschung*, **35,** 23–93.
Palin, R.M., St-Onge, M.R., Waters, D.J., Searle, M.P. & Dyck, B., 2014. Phase equilibria modelling of retrograde amphibole and clinozoisite in mafic eclogite from the Tso Morari northwest India: constraining the P-T–M(H_2O) conditions of exhumation. *Journal of Metamorphic Geology*, **32,** 675–693.
Pilger, A. & Schönenberg, R., 1975. *Geologie der Saualpe, Sonderband 1. Clausthaler Geologische Abhandlungen*. Clausthal-Zellerfeld, 232 pp.
Powell, R. & Holland, T., 1994. Optimal geothermometry and geobarometry. *American Mineralogist*, **79,** 120–133.
Putz, M., Stüwe, K., Jessel, M. & Calcagno, P., 2006. Three-dimensional model and late stage warping of the Plattengneis Shear Zone in the Eastern Alps. *Tectonophysics*, **412,** 87–103.
Roffeis, C., 2008. Bestimmung und Interpretation von vertikalen Druckgradienten über die Plattengneisscherzone (Koralpe, Mittelostalpin). Unpublished MSc thesis, Karl-Franzens Universität Graz, Graz.
Schmid, S.M., Fügenschuh, B., Kissling, E. & Schuster, R., 2004. Tectonic map and overall architecture of the Alpine orogeny. *Eclogae Geologicae Helvetiae*, **97,** 93–117.
Schuster, R., Scharbert, S., Abart, R. & Frank, W., 2001. Permo-Triassic extension and related HT/LP metamorphism in the Austroalpine-Southalpine realm. *Mitteilungen der Geologie und Bergbau Studenten Österreichs*, **44,** 111–141.
Stüwe, K., 1997. Effective bulk composition changes due to cooling: a model predicting complexities in retrograde reaction textures. *Contributions to Mineralogy and Petrology*, **129,** 43–52.
Stüwe, K. & Schuster, R., 2010. Initiation of subduction in the Alps: continent or ocean? *Geology*, **38,** 175–178.
Tenczer, V. & Stüwe, K., 2003. The metamorphic field gradient in the eclogite type locality, Koralpe region, Eastern Alps. *Journal of Metamorphic Geology*, **21,** 377–393.
Tenczer, V., Powell, R. & Stüwe, K., 2006. Evolution of H_2O content in a polymetamorphic terrane: the Plattengneiss Shear Zone (Koralpe, Austria). *Journal of Metamorphic Geology*, **24,** 281–295.
Thöni, M., 2006. Dating eclogite-facies metamorphism in the Eastern Alps – approaches, results, interpretations: a review. *Mineralogy and Petrology*, **88,** 123–148.
Thöni, M. & Jagoutz, E., 1992. Some new aspects of dating eclogites in orogenic belts: Sm-Nd, Rb-Sr, and Pb-Pb isotopic results from the Austroalpine Saualpe and Koralpe type-locality (Carinthia/Styria, southeastern Austria). *Geochimica et Cosmochimica Acta*, **56,** 347–368.
Thöni, M. & Jagoutz, E., 1993. Isotopic constraints for Eoalpine high-P metamorphism in the Austroalpine Nappes of the Eastern Alps: bearing on Alpine orogenesis. *Schweizerische Mineralogische und Petrographische Mitteilungen*, **73,** 177–189.
Thöni, M. & Miller, C., 2009. The "Permian event" in the Eastern European Alps: Sm–Nd and P-T data recorded by multi-stage garnet from the Plankogel unit. *Chemical Geology*, **260,** 20–36.
Thöni, M., Miller, C., Blichert-Toft, J., Whitehouse, M.J., Konzett, J. & Zanetti, A., 2008. Timing of high-pressure metamorphism and exhumation of the eclogite type-locality (Kupplerbrunn–Prickler Halt, Saualpe, south-eastern Austria): constraints from correlations of the Sm–Nd, Lu–Hf, U-Pb and Rb–Sr isotopic systems. *Journal of Metamorphic Geology*, **26,** 561–581.
Von Eynatten, H. & Gaupp, R., 1999. Provenance of Cretaceous synorogenic sandstones in the Eastern Alps; constraints from framework petrography, heavy mineral

analysis and mineral chemistry. *Sedimentary Geology*, **124,** 81–111.

Weissenbach, N., Pilger, N., Schönenberg, R. *et al*. 1978. *Geologische Karte der Saualpe (Kärnten). 1:25.000*. Geologische Bundesanstalt, Wien, 2 Bl.

White, R.W., Powell, R., Holland, T.J.B. & Worley, B.A., 2000. The effect of TiO_2 and Fe_2O_3 on metapelitic assemblages at greenschist and amphibolite facies conditions: mineral equilibria calculations in the system K_2O–FeO–MgO–Al_2O_3–SiO_2–H_2O–TiO_2–Fe_2O_3. *Journal of Metamorphic Geology*, **18,** 497–511.

White, R.W., Powell, R., Holland, T., Johnson, T. & Green, E., 2014a. New mineral activity-composition relations for thermodynamic calculations in metapelitic systems. *Journal of Metamorphic Geology*, **32,** 261–286.

White, R.W., Powell, R. & Johnson, T.E., 2014b. The effect of MnO in metapelitic equilibria revisited: new activity–composition relations and their application to metapelites. *Journal of Metamorphic Geology*, **32,** 808–828.

Whitney, D.L. & Evans, B.W., 2010. Abbreviations for names of rock-forming minerals. *American Mineralogist*, **95,** 185–187.

Wiesinger, M., Neubauer, F. & Handler, R., 2006. Exhumation of the Saualpe eclogite Unit, Eastern Alps: constraints from $^{40}Ar/^{39}Ar$ ages and structural investigations. *Mineralogy and Petrology*, **88,** 149–180.

Wölfler, A., Kurz, W., Fritz, H. & Stüwe, K., 2011. Lateral extrusion in the Eastern Alps revisited: refining the model by thermochronological, sedimentary, and seismic data. *Tectonics*, **30,** TC4006.

Zeh, A., Klemd, R., Buhlmann, S. & Barton, J.M., 2004. Pro- and retrograde P-T evolution of granulites of the Beit Bridge Complex (Limpopo Belt, South Africa): constraints from quantitative phase diagrams and geotectonic implications. *Journal of Metamorphic Geology*, **22,** 79–95.

Received 4 August 2015; revision accepted 10 December 2015.